2s Atomic Level in Muonic ^{208}Pb[†]

D. A. Jenkins and R. J. Powers

Virginia Polytechnic Institute and State University

Blacksburg, Virginia

and

P. Martin, G. H. Miller[††] and R. E. Welsh

College of William and Mary

Williamsburg, Virginia

ABSTRACT

We report the measurement of the energies and the relative intensities of various muonic atomic transitions above 500 keV in ^{208}Pb including transitions to and from the 2s level. Besides the usual E1 transitions we have observed 3d→1s and 4d→2p E2 transitions. Interpretation of these data in terms of various charge distributions is made. Appreciably better fits are obtained by assuming the presence of nuclear polarization and allowing the nuclear polarization parameters $\Delta E(1s)$ and $\Delta E(2s)$ of the 1s and 2s levels to vary. Least squares fits indicate values of $\Delta E(1s) = -8.9 \pm 2.7$ keV and $\Delta E(2s) = -0.6 \pm 0.7$ keV. Comparisons with electron scattering results are made.

[†]Work supported by the National Aeronautics and Space Administration and the National Science Foundation.

[††]National Science Foundation pre-doctoral trainee.

1. Introduction

Traditionally the study of muonic x rays in high Z spherical nuclei has allowed one to characterize the nuclear charge distribution in terms of two parameters.[1] The standard procedure has been to use the $2p \rightarrow 1s$ (K) transitions and $3d \rightarrow 2p$ (L) transitions for information concerning the 1s and 2p muonic levels in order to determine parameters such as the half-density radius and the skin thickness of a Fermi distribution. Transitions between states of higher principal quantum number n, such as the $4f \rightarrow 3d$ (M) transitions, were readily observable but provided essentially no additional information concerning the nucleus and its electromagnetic interactions aside from higher order vacuum polarization effects.[2] Unfortunately this procedure left inaccessible to experimental verification the predicted effects of nuclear polarization by the muon.

The effect a muon bound in an atomic state might have on the charge distribution and vice versa has been the subject of numerous theoretical studies. Originally the increase in binding energy of the 1s muonic state in Pb was predicted to be as large as -60 keV[3] but more recently the predictions have converged[4,5,6] to a value of about -6 keV, an effect readily observable today with solid-state Ge(Li) detectors.

An experimental determination of this quantity is not only important as a check of the theoretical methods involved in the calculations but also essential in the interpretation of muonic x-ray data in terms of the bare or unpolarized nuclear charge distribution unaffected by the presence of the muon. Indeed, one could

make a case that muonic polarization measurements can be used indirectly as a check of theoretical calculations of similar polarization effects in electron scattering by comparing the inferred charge distributions from muonic x rays and electron scattering. These polarization effects have not yet been studied in electron scattering experiments which study nuclear charge distributions.[7]

To determine a third piece of information, i.e. the nuclear polarization, measurements must be made of the energy of a third muon atomic level. The obvious candidate is the 2s level as can be seen from Fig. 1 where we have plotted the linear probability density ϕ of the muon in ^{208}Pb as a function of the radial distance from the center of the nucleus, where

$$\int_0^\infty \phi \, dr = \int_0^\infty (f^2+g^2) r^2 dr = 1 \qquad (1)$$

and f and g are the radial solutions to the Dirac equation.

The drawing includes wave functions for all levels with $n \leq 3$ with the exception of the 3s level, which at present muon intensities seems too weakly populated to be studied. We return to this point in the next section. It is evident from the drawing that the overlap of the 2s level with the nucleus, whose charge distribution is given by the thin line, is second only to the 1s state. The fact that the 2s level is so weakly populated - of the order of 1% that of the 2p levels - has been the reason that the usefulness of this level has been exploited only recently.

Anderson et al[8] first announced observation of the 2s level in heavy muonic atoms reporting one member of each of the 2s→2p and 3p→2s doublets in ^{206}Pb. We[9] later successfully measured the energies of all members of the 3p→2s and 2s→2p doublets in ^{140}Ce.

We have studied the muonic spectrum of ^{208}Pb to see if the transitions not reported in ^{206}Pb could be seen in this isotope of lead. ^{208}Pb has also the merit of being a more theoretically tractable nucleus as it is doubly magic and hence a more attractive test of nuclear matter theories.

Our goal has been to measure precisely as many transitions to and from the 1s, 2s, 2p and 3p muonic levels as possible. We have observed 17 transitions of which 8 are sufficiently well determined to yield useful information concerning the nuclear charge distribution and the nuclear polarization.

As a byproduct of these studies we have also observed several higher order transitions.[10] Beside the normal electric dipole (E1) transitions which are used to determine the nuclear charge parameters, we have observed the electric quadrupole (E2) transitions 4f→2p and 3d→1s. These transitions allow a reasonably direct determination of the relative population of states with the same principal quantum numbers but with different angular momenta. This information has been useful as a check of cascade calculations, made as part of the identification of the less intense dipole transitions to and from the 2s state.

In Section 2 we summarize the theoretical aspects related to muonic ^{208}Pb. Section 3 discusses the experimental apparatus and procedure. The techniques of data analysis appear in Section 4. Section 5 contains the experimental results and a comparison with

other muonic x-ray experiments. Finally in Section 6 we interpret our results in terms of charge distribution parameters and nuclear polarization and compare these with electron scattering data.

The reader must be cautioned that the theoretical interpretation of our data in terms of a two-parameter charge distribution and the nuclear polarization of the 1s level need not be unique. In Section 6 we shall return to this question by examining the sensitivity of our data to different assumptions concerning the charge distribution.

2. Theory

Fig. 2 shows an energy level diagram for muonic ^{208}Pb with a logarithmic scale indicating for each level the relative positions of the eigenvalues of the Dirac equation for a finite distribution of charge (solid lines) and the eigenvalues for a point nucleus (dashed lines). The large finite-size shift for levels with $n \leq 2$ is quite evident. The arrows in Fig. 2 denote the observable electric dipole (E1) transitions.

The solutions to the Dirac equation were obtained using a computer code of McKee[11] which numerically integrates the equation using a Runge-Kutte technique. The eigenvalues have been corrected for vacuum polarization in first order using the theory of Schwinger[12] and in higher order we have included the corrections calculated by Fricke.[13] The Lamb shift including effects due to virtual muon pairs and the anomalous magnetic moment of the muon have been calculated using the procedure of Barrett.[14] In all levels except the 1s we have assumed the values calculated for nuclear polarization by Skardhamar.[6] The choice of this particular set of values to be used

in our fits was prompted by the fact that the calculations in Ref. 6 have been carried out for all muonic states that we have observed. Where comparison is possible there is no significant difference between the calculations of Chen [5] and those of Ref. 6.

In general, we allowed the polarization shift in the 1s level to vary in our fits. Presumably if the experimental value obtained in this experiment agrees reasonably well with the theoretical value, our assumption of the calculated values for the higher levels would be justified. On the other hand, even if the experimental value for the 1s polarization does not confirm the theoretical value precisely, there is reason to believe, as pointed out by Chen[5], that the predictions for the higher levels are more accurate because they include smaller contributions to the polarization from the monopole excitation. It is the monopole modes which contribute heavily to the uncertainty of the 1s level, because of the lack of experimental verification.

For analytical convenience and to allow comparison with electron scattering data[15], we have chosen to parametrize our data in terms of charge distributions expressed in the form of the two generalized Fermi-like functions given below:

$$\rho_1(r) = \rho_0 f_{ncm}(r) [1 + w r^2/c^2]$$
$$\rho_2(r) = \rho_0 f_{ncm}(r) [1 + w r^2 f_{ncm}(r)/c^2] \qquad (2)$$

where $f_{ncm}(r) = [1 + \exp(n^m((r/c)^m - 1))]^{-1}$

In a standard Fermi distribution with w = 0 and m = 1, the parameter c would correspond to a half-density radius and the parameter

n is related to the skin thickness (90% - 10%) t through the relation

$$n = c \ln(81)/ t \qquad (3)$$

A non-zero value for w allows for a central depression or a hump in the charge distribution at the origin. The exponent m allows for a different fall-off of the charge distribution at large distances.

Anticipating the values of one of the charge distributions best-fit by our measured muonic transitions we list typical values for the eigenvalues and the corrections mentioned above. In TABLE 1 we used the charge distribution function $\rho_1(r)$ with $c = 1.1235\ A^{1/3}$ fm, $n = 12.673$, $m \equiv 1$ and $w \equiv 0$. The first two corrections--the first order vacuum polarization and the Lamb shift--were calculated as first order perturbations to the main potential but with finite size wave functions. The remaining two corrections to the energies were taken directly from the literature.[6,13]

As part of our identification of the weak transitions to and from the 2s level we used the observed relative intensities of the muonic x rays. In the long wave length approximation the probability of a bound muon making an Lth order electric (EL) atomic transition is given by[16]:

$$P(EL)_{j\to j'} = 2\alpha m\, c^2/h\ (L+1)/[(2L+1)\ L[(2L-1)!!]^2](\Delta E/m\, c^2)^{2L+1}$$
$$(2j'+1)\begin{pmatrix} j & j' & L \\ \tfrac{1}{2} & -\tfrac{1}{2} & 0 \end{pmatrix}^2 1/(\alpha Z)^{2L}[(Z/a_\mu)^L \int_0^\infty r^L (ff' + gg') r^2\, dr]^2 \qquad (4)$$

where f and g (f' and g') are the initial (final) radial Dirac wave functions for a muon bound to a nucleus with charge Z;

a_μ is the muon Bohr radius;

ΔE is the energy of a muonic transition between atomic states with total angular momenta j and j'.

Following the treatment of Eisenberg and Kessler[17], we have calculated the radiative transition probabilities assuming as the only competing processes Auger K and L electron emission. Using the computer code of Hufner† for atomic levels with $n \geq 4$, we followed the muon cascade beginning at the n = 14 level, assuming that all substates in this level are statistically populated, i.e. proportional to (2j + 1). For all levels with $n > 4$ point-nucleus atomic wave functions were used to calculate the radial matrix elements and point nucleus transition energies ΔE were employed. For $n \leq 4$ we solved the Dirac equation to obtain the radial matrix elements assuming the Fermi distribution ρ_1 with the same parameters given above. We used our measured energies for these lower transitions which we observed. Otherwise we used the finite nucleus eigenvalues calculated using the above parameters. The calculations took account of both E1 and E2 radiative transitions for all levels for $n \leq 5$. However, only the 4f→2p and 3d→1s transitions were intense enough to be observed.

E2 transitions can be observed in muonic atoms of high Z when it is possible for a muon to make an energetically favored E2 transition with a change in principal quantum number $\Delta n > 1$ instead of an E1 transition with n=1. For example, the calculated

†The cascade calculations for a point distribution were made with a program supplied by J. Hufner as modified by G. Hunt.

value of the ratio R of de-excitation intensities from the 3d atomic state via E1 and E2 transitions is given (using non-relativistic wave functions for a point nuclear charge distribution) by

$$R(E1/E2) = P(3d\rightarrow 2p)/\, P(3d\rightarrow 1s) = 15/\,(Z\alpha)^2 \qquad (5)$$
$$= 42. \text{ for } {}^{208}\text{Pb}.$$

Using relativistic wave functions for a finite distribution of nuclear charge we find that the predicted ratio R decreases by more than a factor of 2 to 20.4. Indeed, such E2 transitions from circular orbits ($\ell = n - 1$) can be of comparable intensity to E1 transitions from inner orbits ($\ell < n - 1$) which are much less populated than the circular orbits. Consider the theoretical populations of the muonic atomic levels in ^{208}Pb given in TABLE 2. Although the E1 transition rate from the 3p level to the 1s level is considerably faster than the E2 de-excitation rate from the 3d level to the 1s level by more than an order of magnitude, the high population of the 3d level relative to the 3p level actually predicts more intense 3d→1s E2 transitions than the 3p→1s E1 transitions. Notice that the 3s level is predicted to be less than one-fifth as highly populated as the 2s level, which itself is occupied 1.6% of the time. Observation of the 3s and 4s levels was beyond the statistics of this experiment.

In light of the fact that our intensity predictions are intended only as a secondary verification of our identification of the weak atomic transitions, we neglected two effects which will quantitatively affect the predictions. First we neglected such radiationless transitions as prompt neutron emission observed by

Hargrove et al.[18] This mechanism could produce a depopulation of some of the levels with $n \geq 3$. Experiments performed at the Chicago synchrocyclotron suggest that these effects could be as large as 10%. Secondly, for precise calculations in high Z muonic atoms, the long wave length approximation used in this discussion should be replaced by the exact expression[19] containing spherical Bessel functions resulting from the multipole expansion of the vector potential. In spite of these approximations, we find reasonably good agreement between observed and predicted relative intensities.

3. Experimental Details

3.1 Beam and Apparatus

The data for this experiment were collected during two experimental periods at the 600 MeV synchrocyclotron of the N.A.S.A. Space Radiation Effects Laboratory (SREL) in Newport News, Virginia. A low duty-factor beam was produced with a thin carbon filament ''harp'' as an internal target.

The prime experimental concern has been the measurement of energies of transitions to and from the muonic 2s state. Since these are of low intensity, we used the backward beam transported by the SREL meson channel in order to obtain the best possible signal-to-noise ratio. A previous muonic x-ray experiment with ^{140}Ce had shown that although the forward beam had twice the particle intensity, there was also greater contamination.[9] Use of the backward muon beam improved the signal-to-noise ratio from 2:1 to 3.5: 1 at 4.2 MeV (^{140}Ce K lines) and from 5:1 to 8.5:1 at 1.3 MeV (^{140}Ce L lines).

A standard beam telescope was used as is shown in profile in Fig. 3. Counters 1 and 2 served as a beam monitor. Counter 3, which was adjacent to and the same size as the target, defined muons incident on the target. Counter 4 was a large anti-coincidence counter used to define a stop and counter 5 served to monitor the efficiency of 4. Under proper operating conditions counter 4 was about 98.5% efficient as determined by the ratio $(1235)/(123\bar{4}5)$. A stopping muon was signified by concident signals from counters 1,2 and 3 with no signal from 4, i.e. $(123\bar{4})$. Because our range curve indicated less than a 5% electron contamination, we used no Cerenkov counter to veto electrons. Muon stopping rates were typically 25 k/s.

Precautions were taken to exclude high Z material from the region of the gamma ray detector. The shielding consisted exclusively of borated CH_2 and the frame supporting the counters was constructed of Al. The nearest Pb,aside from the target, was in the 20 cm x 20 cm beam collimator, which was 1 m upstream from the target. The beam was moderated with 25 cm x 25 cm polyethylene sheets which were inserted downstream of counter 2. The photon detector was placed centrally under the target and was kept beneath the beam level in order to minimize beam-rate effects. A typical singles rate in the detector was 2000 counts per second. The detector was a 7% efficient, coaxially-drifted Ge(Li) detector (Princeton Gamma Tech). Under operating conditions this detector exhibited a resolution of 3.2 keV at 1.3 MeV (^{60}Co) and 3.6 keV at 2.6 MeV (^{56}Co).

The detailed composition of the target and its dimensions are shown in TABLE 3. The target was $Pb(NO_3)_2$ powder placed in a

rectangular box made from thin plastic sheets.

3.2 Electronics

We collected essentially two pieces of information during the experiment: the pulse height of the γ ray in the detector and the timing of the γ ray relative to a muon stopping within 500 ns. In this discussion the term γ ray will be used to mean either a nuclear γ ray or a muonic atomic x ray. These two dimensional spectra allowed us to distinguish between prompt events such as a muonic x ray, where the muon stop and the subsequent atomic x ray are experimentally instantaneous, and delayed events such as nuclear γ rays resulting from muon capture.

Both pieces of information were fed into Analog to Digital Converters (ADC) which were gated on after a γ-stop coincidence had been detected. Fig. 4 shows the main logic circuitry used in analyzing the signals. The stopped muon signal ($123\bar{4}$) was obtained from the usual combination of discriminators, delays and coincidence units. The signal from the detector was initially passed through a room-temperature FET preamplifier (Canberra 1408C) which also received a signal from a reference pulser used for stabilization. The pulser signal was fed to the first preamplifier stage through a 1.5 pf precision capacitor which had a temperature stability of 1 part in 10^6 per degree centigrade. Preamplifier signals were fed to the main amplifier system which consisted of a Tennelec TC200 amplifier and a Tennelec TC203 Linear Amplifier, where the pulses were shaped and pole-zero and baseline restorations were applied, before energy analysis. Two additional Stage 1 outputs from the

TC200 were fed into discriminators and then recombined in a coincidence unit to extract a timing signal for the pulse. One discriminator was set to trigger above the noise and was given a wide output, while the other triggered in the noise but had a narrow, slightly delayed output. Thus an output from the coincidence unit denoted a signal whose magnitude was above the noise but yet could be given,effectively,leading edge timing. Using this method we obtained a timing resolution of 100 ns full width at half maximum (FWHM) over an energy region from 0.1 to 8.5 MeV. Outputs from this coincidence unit were used as one input to the γ-stop coincidence unit and as the ''START'' signal of the time-to-amplitude converter (TAC), which served to provide an analog signal giving the time delay between a stopping muon and the resultant γ rays. The other input to the γ-stop coincidence unit, and the ''STOP'' signal of the TAC were provided from discriminator outputs of a delayed ($123\bar{4}$). The γ-stop coincidence provided a gating signal for both the energy and timing ADC's. Incorporated into the γ-stop coincidence unit was an anti-coincidence signal formed when either of the ADC's was busy or when incoming signal rates became too high. The latter was produced by a commercial pile-up protector. The γ-stop coincidence unit could also be gated off by a pulse derived from the synchrocyclotron R.F. signal during the prompt beam ''spike''.

The services of the data acquisition facilities of the SREL IBM 360-44 were not continuously available to us and thus a variety of data accumulation techniques was employed. When the computer was unavailable the timing information was analyzed in a 400 channel

(T.M.C.) analyzer. When we were ''running on-line'' with the computer a 1024 channel ADC (Kicksort) was used, and the output fed directly into the computer via the IBM 2972/7 interface. The analog energy signal from the TC203 was fed into a 8192 (Kicksort) channel pulse height analyzer (PHA), which could be used with or without the computer. Since this PHA memory had only 4096 channels it was necessary to accumulate separately into the upper and lower halves of the energy region studied when ''running off-line''. When the computer was available, 13 bits of energy information and 10 bits of timing information, for each valid event, were transferred to the computer and stored there.

A block diagram of the data flow is shown in Fig. 5. For each valid event, the timing and energy information were transferred through the IBM 2972/7 Interface to the computer. The computer was used to analyze these data into two 8192 channel energy arrays, one prompt and the other delayed with respect to a muon stop signal, and one 1024 channel timing array. In addition cumulative prompt and delayed energy analyzers were kept in disk storage. All of these arrays were continuously monitored during each run via printer, X-Y plotter and cathode-ray display. The timing windows for separating the prompt and delayed spectra were established by inspecting the timing spectrum over the whole energy range and visually judging where the exponential decay commenced, (Fig. 6). When accumulating data without the on-line computing facilities, we adjusted the timing so that the energy P.H.A. would accept signals during 100 ns for each muon stop. These stored data were initially printed out on a high speed

paper printer, but during the last run an incremental magnetic tape unit (Cipher) was used to store the energy and timing information for each event, and to record the contents of the 4096 channel energy analyzer memory.

C. Experimental Methods

In order to ensure run-to-run consistency a two-point digital stabilizer (Kicksort) was used in conjunction with the energy ADC. This held fixed the centers of the two chosen peaks by applying corrections to the gain and slope intercept of the energy ADC. The two lines used for stabilization were the 511 keV line from positron annihilation and a reference pulser peak. The high stability precision reference pulser was constructed from the design of M.G.Strauss at Argonne[20]. The voltage of the reference pulser was adjusted to be equivalent to an 8.2 MeV γ ray. This was chosen since it gave a very large energy spread for stabilization and kept the stored reference pulses clear of the prominent muonic lines. The pair of stabilization lines had the further advantage of being easily included in calibrations, and hence there was no danger of gain changes during calibrations.

The usual experimental sequence involved collecting data from a target for 7-10 hours, with a short calibration run directly preceding and following each run. The beam was left on during calibration runs but in order to speed data collection the ''STOP'' requirement of the ''γ-stop'' coincidence unit was removed, and the data collected was ''self-gated.'' The main purpose of these calibration runs was to verify that there had been no substantial gain shift during the target run which might cause peak broadening

with a resultant loss of resolution. Once it became apparent that the system was extremely stable, the calibration runs were taken less frequently and the target runs extended in duration.

The absolute energies of the muonic transitions were determined using two techniques. The energies of prominent transitions, such as the K, L and M lines were evaluated using a ''feed-through'' technique, whereby muonic peaks and precisely known calibration peaks were accumulated simultaneously. Several calibration sources whose energies are accurately known and which lie close in energy to the muonic transition of interest were chosen. The sources were then placed near the detector and appeared in the muonic spectrum by accidental coincidences with muon ''STOP'' signals. Experimentally this technique was convenient since the data accumulate sufficiently rapidly that a fit to the lines from one eight hour run was not statistically limited. A sample spectrum illustrating this technique to determine the L energies is given in Fig. 7. In this case lines from ^{24}Na and ^{208}Tl were used for calibration sources. In the case of a weak calibration source, such as ^{66}Ga (used to evaluate the K lines), this technique had to be amended by removing the requirement of a ''STOP'' signal, thus permitting more rapid data accumulation of the calibration peaks. Checks were made to search for a possible dependence of the measured energy on the mode of data collection. Provided the deadtime of the PHA was kept within reasonable limits (25% deadtime), any difference was well within statistical error, independent of whether the beam was on or whether a photon occurred in coincidence with a muon stop.

In most ''feed-through'' runs the chosen calibration lines were within 100 keV of the muonic transitions to be measured. TABLE 4 lists the calibration sources used and their energies. To evaluate the transition energy we assumed the system was linear over the small range of interest. A justification for the validity of this technique was the good consistency found when a line was evaluated from more than one pair of calibration lines and at different gain settings.

The remaining muonic transition energies such as the $2s \rightarrow 2p$ transitions were determined relative to the prominent transitions in the summed spectrum using the gain curve determined in the calibration runs. This is further discussed in the next section.

4. Data Analysis

All peaks in both prompt and delayed spectra were analyzed using a least squares fitting technique. Since most of the peaks corresponded to γ rays whose natural width were less than our experimental resolution, the mathematical form of the line shape should represent the response of the apparatus and should be Gaussian.

If $N_i(x)$ represents the theoretical number of counts in channel x, contributed by the i^{th} Gaussian (allowing for the presence of more than one peak in the neighborhood of channel x), then the theoretical form assigned to it was:

$$N_i(x) = A_i \exp(-(x-X_i)^2/2(k\omega_i)^2), \qquad (6)$$

and the form of the complete function was

$$N_{th}(x) = \sum_{i=1}^{j} N_i(x) + \text{Background}. \qquad (7)$$

In these formulae

$k = 2.35498$

X_i = central channel of i^{th} Gaussian

A_i = amplitude in counts of the i^{th} Gaussian

ω_i = full width at half maximum in channels of the i^{th} Gaussian.

In practice the maximum number of Gaussians j, was restricted to 4, and in general the number of variables was reduced by equating all the widths ω_i to a single variable ω.

Using this mathematical form, the observed intensity I_i of the transition is given by the area under the Gaussian.

$$I_i = k\ \omega_i\ A_i/\sqrt{\pi} \qquad (8)$$

In order to be able to represent both backgrounds with finite curvature and linear backgrounds an exponential function was assumed:

$$\text{Background} = B\ \exp[\lambda(x-X_1)]$$

where

B = amplitude of background at the center of Gaussian 1

λ = variable exponential constant.

It was found that varying the number of channels over which this function was fitted did not appreciably affect the values of the parameters derived (A_i, X_i, ω_i, B, λ), provided the range was large enough to allow a good fit to the background function. Exceptions occurred in cases where structure from another Gaussian was obviously being included in the range. As a rule these tech-

niques gave a variance between 0.5 and 1.5, indicating a good theoretical representation had been used for the data.

Prior to one of the runs the detector sustained some neutron damage and this resulted in exponential tails on the Gaussians, due to incomplete collection of charge. For these data the variances for a Gaussian function were very much larger and in order to fit the data properly a mathematical form of the type suggested by Routti and Proussin[24] was used. This allowed two additional parameters, transition points beyond which the Gaussian function became a decaying exponential, while still preserving functional and differential continuity at the boundaries. For this function

$$N_i(\chi) = \begin{cases} A_i \exp[-(x-X_i)^2/2(k\omega_i)^2] & \\ \qquad \text{for } X_i - v^2 \le x \le X_i + u^2 & \\ A_i \exp[-v^2(2x-2X_i + v^2)/2(k\omega_i)^2] & \\ \qquad \text{for } x < X_i - v^2 & \\ A_i \exp[-u^2(2X_i-2x + u^2)/2(k\omega_i)^2] & \\ \qquad \text{for } x > X_i + u^2 & \end{cases} \tag{9}$$

where v^2 and u^2 are the distances below and above the central channel at which exponential behavior starts. The same functional form was always used to analyze both calibration and data runs, and in all cases the uncertainties quoted are one statistical standard deviation.

Transitions involving the 2s state, as well as many of the other higher transitions, were relatively weak and hence completely unobservable or at best statistically limited in one ten hour run. Some method was thus required for summing the data while not obscuring any peaks. Simple adding was insufficient since the runs on each

target extended for two weeks or more and typical daily gain variations were 50 parts per million as determined from the calibration runs. To compensate for this, one run was chosen as the ''basis'' run, either because there was a calibration source feeding through on accidental coincidences, or because of high consistency between the pre- and post-calibration runs. Within the ''basis'' run two well defined peaks were chosen and their centers determined. These same two peaks were fitted in each run which was to be summed. If y_1 and y_2 are the peak centers in the ''basis'' run and c_1 and c_2 are the same peak centers in the run to be summed, then the linear transformation

$$ch(b) = m\, ch(r) + k \qquad (10)$$

where $ch(b)$ is a channel in the ''basis'' run,

$ch(r)$ is a channel in the run to be summed,

$m = (y_1 - y_2)/(c_1 - c_2)$

and $k = c_1 - m y_1$,

will map the centers c_1 and c_2 onto y_1 and y_2 respectively. Using this transformation we determined what fraction of any run's channels contributed to a given channel in the ''basis'' run. After each run was mapped onto the ''basis'' run, the channels were summed. The data were then in the form of two 8182 channel arrays (corresponding to prompt and delayed spectra) in which the energies of the dominant peaks were accurately determined from ''feed-through'' runs. From these summed data and using source calibration runs to determine the linearity, we evaluated the energies of the weaker transitions relative to the ^{208}Pb M lines and the ^{208}Pb L and K lines

(full energy, single escape and double escape peaks†). In all we used 14 peaks in our summed spectra as ''primary standards'' with which to determine the weaker transitions.

The linearity was determined using the ^{56}Co, ^{22}Na and 511 keV annihilation lines given in TABLE 4. It proved convenient to fit these 14 lines to a third order polynomial, a functional form that gave reasonable fits to the linearity data.

As a check of our summing techniques and our knowledge of the linearity of the system, we collected data at two gain settings: 0.68 keV/channel and 1.1 keV/channel. In general, the consistency of the measured energies between gain settings was reasonable, since the lines of interest were close to one of the ''primary standard'' peaks. The few inconsistencies were taken into consideration by increasing the quoted errors to allow for any possible local uncertainty in the linearity.

5. Experimental Results

5.1 Energies

In TABLES 5 and 6 we list the energies of the well-established E1 and E2 muonic transitions and related splittings for ^{208}Pb. In general the splittings are more accurately determined because an absolute calibration is not needed. For comparison we include the results of the Chicago-Ottawa[8] collaboration and those of CERN[2].

†Ref. 25 has verified that the energy difference of the full energy and double escape peaks as observed in a coaxial Ge(Li) is twice the electron rest mass to within 0.08 keV.

In general there is excellent agreement where comparisons are possible. In the last column of each table we list the theoretical predictions assuming a two-parameter Fermi distribution for the charge density anticipating the values for c and n obtained in our least squares fit.

The identification of the weaker observed transitions and the absence of others from TABLE 5 deserve some discussion. Fig. 8 shows the high-gain muonic spectra in the region of the 2s→2p transitions for both prompt and delayed times. The delayed spectrum has been enhanced by using a timing window approximately four times the prompt-time window. The $2s_{1/2} \rightarrow 2p_{3/2}$ transition appears in an energy region which is relatively free from background radiation. However, in the region of the $2s_{1/2} \rightarrow 2p_{1/2}$ transition we find two γ rays, one of which appears with almost equal intensity in the prompt and delayed spectra with an energy of 1207.89 ± 0.50 keV. This line has been tentatively identified as the 1230. ± 30. keV transition[26] in ^{207}Tl connecting the 2.92 ± 0.02 MeV ($?^-$) state to the 1.69 ± 0.02 MeV ($5/2^+$) state. The strong delayed component of this γ ray would be consistent with a muon capture process which would produce ^{207}Tl. The 2p splitting Δ2p, known from the K splitting, is used to verify that the remaining line is the $2s_{1/2} \rightarrow 2p_{1/2}$ transition. As can be seen from TABLE 6 there is excellent agreement between Δ2p determined from the 2p→1s transitions and that determined by the 2s→2p transitions. As shall be discussed in the next section the relative intensity of these peaks will be used to confirm the identification.

As an additional check of our determination of the 2s level we had hoped to identify both 3p→2s transitions which bracket the double escape peak of the $3d_{5/2}\rightarrow 2p_{3/2}$ transition. Unfortunately we were able to identify unambiguously only the $3p_{3/2}\rightarrow 2s_{1/2}$ transition. In the region of the $3p_{1/2}\rightarrow 2s_{1/2}$ transition there was too much structure and background to yield consistent energies between the high and low gain runs. We have tentatively identified one line in this region as the 1310 ± 30 keV transition[26] connecting the 3.00±0.02 MeV ($?^-$) level to the 1.69±0.02 MeV ($5/2^+$) in ^{207}Tl. As a result we have included only the $3p_{3/2}\rightarrow 2s_{1/2}$ transition in our interpretation. The justification for its identification will be based on its relative intensity and the consistency of its energy with other transitions involving the 2s level.

Figs. 9 and 10 show our fits for the E2 transitions, 4f→2p and 3d→1s. The latter transitions were remarkably free of unidentifiable structure whereas there seemed to be some structure just below the $4d_{3/2}\rightarrow 2p_{1/2}$ transition. The rapid suppression of the E2 rate as the principal quantum number increases is clearly seen. Whereas the 3d→1s transitions are nearly twice as intense as the 3p→1s transitions, the 4f→2p transitions are only half as intense as the 4d→2p and there was no evidence at all for the 5g→3d transitions.

Because we have overdetermined many of the energy levels by observing more than one transition to or from a given energy level, it is possible to determine the internal consistency of our experimental results.For instance, the energy difference between the $3p_{3/2}$ and $2p_{1/2}$ levels can be inferred by combining the energies of the $3p_{3/2}\rightarrow 2s_{1/2}$ and $2s_{1/2}\rightarrow 2p_{1/2}$ transitions or by adding the energy of the $3d_{3/2}\rightarrow 2p_{1/2}$ transition to the splitting $\Delta(3p_{3/2}\text{-}3d_{5/2})$

between the $3d_{5/2} \rightarrow 1s_{1/2}$ and $3p_{3/2} \rightarrow 1s_{1/2}$ lines and $\Delta 3d$ inferred from the two lower energy L transitions. The comparisons involving the 2s level are given in TABLE 7. The quoted error of the energy sum is simply the sum of the individual errors added in quadrature. In both cases the discrepancy is well within twice the error of the least-accurate compounded energy. It is interesting to note that in the course of our least-squares fits to charge parameters the measured value of $\Delta(3p_{3/2}-3d_{5/2})$ was consistently two standard deviations low. This fact by itself would explain the slight discrepancies indicated in TABLE 7.

As an additional check we studied ^{206}Pb to observe the 3d→1s transitions. A comparison of the fine structure splittings in this energy region shows excellent agreement between theory and experiment. This strengthens the hypothesis that the low value of $\Delta(3p_{3/2} - 3d_{5/2})$ in ^{208}Pb is nothing but a statistical fluctuation.

5.2 Relative Intensities

As confirmation of our identification of the less intense transitions to and from the 2s level we have measured the relative intensities of all muonic transitions between 900 keV through 3400 keV. The relative efficiency of the Ge(Li) detector was measured using a ^{56}Co source and the relative intensities of its gamma rays ranging in energy from 834 keV to 3250 keV given by Scott and Van Patter[23]. Effects due to the attenuation of the muonic x rays inside the target were calculated using the Los Alamos[27] tabulation of the mass absorption coefficients.

TABLE 8 gives a comparison of our observed relative intensities with those predictions obtained via the assumptions given in Section 2. The errors represent a combination of the uncertainty of the number of counts in each peak and our estimate of the uncertainty of the relative efficiency of the detector. The experimental numbers have been arbitrarily normalized to give agreement with $3d_{5/2} \rightarrow 2p_{3/2}$ and $4f_{5/2} \rightarrow 3d_{3/2}$ transitions. Over all there is moderately good agreement, particularly in light of the approximations made in Section 2. Especially encouraging is the excellent agreement between theory and experiment of the 4f→2p E2 transitions. One point worth noting is that the transitions to and from the 2s level are uniformly weaker than predicted (but by no more than three standard deviations). The suggestion has been made by Srinavasan and Sundaresin[28] that a muon in an np state ($n \geq 3$) can de-excite by emission of a prompt neutron. Such prompt neutron emission has already been observed[18] as mentioned above. They predict the ratio of the non-radiative to the radiative transition rate to be of the order of 0.6. This would explain at least in part the decreased intensity of the $3p_{3/2} \rightarrow 2s_{1/2}$ transition and consequently the decreased 2s→2p intensities. We shall return to this point below where we discuss the relative intensities of the 3p→1s transitions.

A closer examination of the fine structure intensity ratios does reveal some very real anomalies which we are unable to explain using the simplified cascade theory given in Section 2. In TABLE 9 we show a comparison between the observed fine structure intensity ratios for the M, L and K transitions with those of the

Chicago-Ottawa collaboration and theory. There is quite excellent agreement between the two experiments but neither agrees well with the theory, particularly the L transitions. An extrapolation of our detector efficiency from 3200 keV to 6000 keV reveals an intensity prediction for the $2p_{1/2} \rightarrow 1s_{1/2}$ transition in moderate agreement with theory and suggesting that the $2p_{3/2}$ level is underpopulated. The anomaly in the L transitions could similarly be explained by an underpopulation of the $3d_{5/2}$ level.

Finally we show in TABLE 10 the relative intensities of the E1 and E2 transitions in the energy regions of the 4d→2p and the 3p→1s transitions. It is interesting to note the quite excellent agreement between theory and observation with the sole exception of the $3p_{3/2}$ level in ^{208}Pb, which is four standard deviations low. Preliminary analysis of muonic x rays in ^{206}Pb shows no such anomaly. It is true that prompt neutron emission would allow for a depopulation of both 3p levels of the same order of magnitude as that observed in the $3p_{3/2}$ level in ^{208}Pb. However, the $3p_{1/2}$ level in ^{208}Pb seems unaffected. We presently know of no mechanism which would preferentially depopulate the $3p_{3/2}$ level relative to the $3p_{1/2}$.

In conclusion we feel that the moderate agreement of the relative intensities of the weak transitions confirms our identification of these peaks.

6. Discussion of Results

We have interpreted our results in terms of nuclear charge parameters and nuclear polarization information. We treat first

the question of polarization by assuming a simple two-parameter Fermi distribution. We shall then discuss the possibility of other distributions and compare our findings with those from electron scattering[15]. Initially we shall assume no uncertainty in the theoretical calculations and that the sole source of error is the experimental data. We shall examine this assumption later.

We have selected the eight transitions marked with an asterisk in TABLE 8 and $\Delta 2p$ obtained from the K_α splitting to be used in our least-squares fits to various charge distributions. Our criteria for limiting our choice to these data was i) sensitivity to finite size effects and ii) accuracy. Essentially we included all data affected by the 1s, 2s, 2p or 3p levels as long as they were well enough determined to contribute usefully to the fit. We arbitrarily eliminated from our fits those transitions whose errors were greater than 0.8 keV. The inclusion of such data, in general, yielded results compatible with the fits from the ''basic nine'' data but the larger errors tended to artificially lower the χ^2. $\Delta 2p$ was included in the fit as it was measured independently of the K_α feed-throughs and was significantly more accurate than the K_α lines. It was determined from the 511 keV energy differences of the full-energy, single-escape and double-escape K_α peaks.

In TABLE 11 we give the results of least-squares fits of the selected data to a two-parameter Fermi distribution $\rho_1(r)$ given in Eq.2 assuming, i) no nuclear polarization, ii) the values of nuclear polarization calculated by Skardhamar[6] and iii) the values of Skardhamar except for the polarization $\Delta E(1s)$ in the 1s level, which was allowed to vary. The relative quality of the three fits as indicated by the χ^2 per degree of freedom (χ^2/DF)

indicates quite dramatically that assumption iii yields an appreciably better fit.

TABLE 12 gives some three-parameter fits using $\rho_1(r)$ and $\rho_2(r)$ and allowing $\Delta E(1s)$ to vary. The fixed values for w and m were taken from some of the fits given by Heisenberg et al.[15] to electron scattering and other muonic x-ray data. It is clear that we cannot choose between any of the forms as giving a better fit. Indeed, all four distributions give quite acceptable χ^2. However, it is interesting to note that they all give essentially the same value for $\Delta E(1s)$. Admittedly these four distributions do not exhaust all possible distributions but they are fairly representative of the simpler analytic forms that have been used in charge distribution analyses. In Fig. 11 we plot the first three distributions for comparison. The insensitivity of the transitions used in the fit to such features as the central depression is demonstrated by the fact that all these distributions are fitted equally well.

The value for $\Delta E(1s) = -12.5 \pm 0.8$ keV is to be compared with those theoretical values of -6.8 ± 2.0 keV and -6.0 ± 0.6 keV of Skardhamar[6] and Chen[5] respectively. This discrepancy between our experimental value and that predicted by theory led us to reexamine our assumption of Skardhamar's values for the higher levels. Since the monopole contribution to $\Delta E(1s)$ is the source of the largest uncertainty, this uncertainty should affect all other s states, in particular the 2s level. As a result we tried four parameter fits for c, n, $\Delta E(1s)$ and $\Delta E(2s)$ using the same distributions given in TABLE 12. It is legitimate to try

to fit a fourth parameter as we have observed transitions from the $3p_{3/2}$ level which has a finite size effect of 85 keV. Our results are summarized in TABLE 13. Again the observed values for $\Delta E(1s)$ and $\Delta E(2s)$ are fairly independent of the assumed charge distribution. The effect of allowing $\Delta E(2s)$ to vary is to lower the fitted value of $\Delta E(1s)$.

As mentioned earlier, we have considered only the experimental uncertainty as a possible source of error in the above fits. If we include the theoretical uncertainties in the nuclear polarization for all levels other than the 1s and 2s levels as given by Skardhamar as well as the uncertainty induced by using different distributions we obtain the values found in TABLE 14 for the polarization of the 1s and 2s levels obtained from a four-parameter fit to our data. We include the theoretical values for comparison. We find quite good agreement between theoretical and experimental values for $\Delta E(1s)$ and $\Delta E(2s)$.

Finally we compare some of our fits to equivalent fits of electron scattering data in TABLE 15. In the second column is our three-parameter fit assuming a distribution $\rho_1(r)$ with variable c, n, $\Delta E(1s)$ and $\Delta E(2s)$. To permit comparison we have adopted the value and error for w found by Bellicard and van Oostrum[29] in their three-parameter fit to 175-250 MeV electron data. We also include a comparison of a fit to 250 MeV data[15] assuming a four parameter distribution $\rho_1(r)$. In both cases there seems to be good agreement with electron scattering data, although an assessment of this agreement is premature as the nuclear polarization effects on the ^{208}Pb electron scattering data have not yet been included

in the analyses.[30]

In summary we feel our data strongly demonstrate the presence of nuclear polarization effects in muonic ^{208}Pb. This is borne out by our significantly better fits allowing for nuclear polarization than those obtained assuming no nuclear polarization. Our inferred values of the polarization in both the 1s and 2s levels agree quite well with theory. We repeat our initial warning that the inferred values for E(1s) and E(2s) could conceivably be model dependent. But we have found no such indication of this from the charge distributions we have examined.

7. Acknowledgements

We wish to thank Profs. K. Ford, D. G. Ravenhall, D. Wilkinson and L. Wilets for helpful discussions of our data. We appreciate the hospitality of Dr. R. T. Siegel and the staff of the Space Radiation Effects Laboratory. We are grateful to Mr. R. Hart for his diligent programming help with the data analysis. We appreciate the loan of the separated ^{208}Pb by Drs. G. Rogosa and E. Ritter.

References

1. C. S. Wu and L. Wilets, Ann. Rev. Nucl. Sci. 19, (1969), 527

2. G. Backenstoss, S. Charalambus, H. Daniel, Ch. von der Malsburg, G. Poelz, H. P. Povel, H. Schmitt and L. Tauscher, Phys. Lett. 31B, (1970) 233.

3. L. N. Cooper and E. M. Henley, Phys. Rev. 92 (1953) 801.

4. R. K. Cole, Jr., Phys. Rev. 177 (1969) 164.

5. M. Chen, Phys. Rev. C1, (1970) 1167; Thesis (Princeton University - 1969).

6. H. F. Skardhamar, Nucl. Phys. A151 (1970) 154.

7. G. H. Rawitscher, Phys. Lett. 33B (1970) 445.

8. H. L. Anderson, C. K. Hargrove, E. P. Hincks, J. D. McAndrew, R. J. McKee, R. D. Barton and D. Kessler, Phys. Rev. 187 (1969) 1565.

9. D. A. Jenkins, R. J. Powers, P. Martin, G. H. Miller, R. E. Welsh, and A. R. Kunselman, Phys. Lett. 32B (1970) 267.

10. P. Martin, G. H. Miller, R. E. Welsh, D. A. Jenkins and R. J. Powers, Phys. Rev. Lett. 25 (1970) 1406.

11. R. J. McKee, Phys. Rev. 180 (1969) 1139.

12. J. Schwinger, Phys. Rev. 75 (1949) 651.

13. B. Fricke, private communication; see also B. Fricke, Z. Phys. 218 (1965) 495.

14. R. C. Barrett, S. J. Brodsky, G. W. Ericson, and M. H. Goldhaber, Phys. Rev. 166 (1968) 1589.

15. J. Heisenberg, R. Hofstadter, J. S. McCarthy, I. Sick, B. C. Clark, R. Herman and D. G. Ravenhall, Phys. Rev. Lett. 23 (1969) 1402.

16. S. Devons and I. Duerdoth, Advan, Nucl. Phys. 2 (1968) 340.

17. Y. Eisenberg and D. Kessler, Nuovo Cimento 57B (1968) 235.

18. C. K. Hargrove, E. P. Hincks, G. R. Mason, R. J. McKee, D. Kessler, and S. Ricci, Phys. Rev. Lett. 23, (1969) 215.

19. M. E. Rose, Elementary Theory of Angular Momentum (Wiley, New York, 1957), Chap. Vii.

20. M. G. Strauss, L. L. Sifter, F. R. Lenkszus and R. Brenner, IEEE Trans. Nucl. Sci. Vol. NS-13, 3(1968).

21. C. M. Lederer, J. M. Hollander, and I. Perlman, Table of Isotopes, 6th Edition, (New York: John Wiley & Sons, Inc.) 1967.

22. M. G. Strauss and F. R. Lenkszus, Nucl. Phys. A 132 (1969) 195.

23. H. L. Scott and D. M. Van Patter, Phys. Rev., 184 (1969) 1111.

24. J. T. Routti and S. G. Prussin, Nucl. Inst. and Meth. 72 (1969) 125.

25. M. G. Strauss, F. R. Lenkszus and J. J. Eichholz, Nucl. Instr. and Meth. 76 (1969) 285.

26. O. Hansen and O. Nathan, Nucl. Phys. A127, (1969) 71.

27. Los Alamos Report LA-3753-Photon Cross Sections from 0.001 to 100 MeV for Elements 1 through 100.

28. V. Srinivasan and M. K. Sundaresan (to be published).

29. J. B. Bellicard and K. J. van Oostrum, Phys. Rev. Lett. 19, (1967) 242.

30. J. Heisenberg, R. Hofstadter, J. S. McCarthy, I. Sick, M. R. Yearian, B. C. Clark, R. Herman and D. G. Ravenhall (to be published).

Figure Captions

Fig. 1. Linear probability density $(ff^* + gg^*)r^2$ as a function of radius for muonic ^{208}Pb 1s, 2s, 2p, 3p and 3d states. For comparison the unlabelled thin curve depicts the charge distribution for the ^{208}Pb nucleus assuming a slight central depression of 0.14.

Fig. 2. Muonic energy levels in ^{208}Pb showing observed E1 transitions. The heavy lines represent the actual level energy including finite-size effects. The dashed lines indicate the level energy for a point distribution of charge.

Fig. 3 Profile view of the stops telescope and the geometry of the Ge(Li) detector.

Fig. 4. Schematic diagram of the electronics logic.

Fig. 5. Schematic diagram of data flow. The circled numbers indicate alternate paths depending on whether ''on-line'' or ''off-line'' data collection techniques were used.

Fig. 6. Timing spectrum of muonic ^{208}Pb events relative to the muon stop. The direction of increasing time is to the left of the drawing. The peak at the right indicates γ-rays ''prompt'' or in time with the muon stop.

Fig. 7. L muonic x rays in ^{208}Pb with accidental feed throughs of ^{208}Tl and ^{24}Na calibration lines at 0.68 keV per channel.

Fig. 8. Prompt and delayed spectra of 2s → 2p transitions in ^{208}Pb. The timing window for the delayed events is four times that of the prompt events at 0.68 keV per channel.

Fig. 9. 4d → 2p and 4f → 2p transitions in muonic ^{208}Pb. The dashed line indicates a fitted background. The vertical bars indicate the relative intensities of the lines. Both prompt and delayed spectra are shown with equal timing windows.

Fig. 10. 3d → 1s and 3p → 1s atomic transitions in muonic ^{208}Pb. The dashed line indicates a fitted background. The vertical bars indicate the relative intensities of the lines. Both prompt and delayed spectra are shown with equal timing windows.

Fig. 11. Comparison of ^{208}Pb charge densities fitted to our data. The numbers refer to the distributions given in TABLE 12.

TABLE 1

MUONIC ENERGY LEVELS IN ^{208}Pb
(keV)[e]

MUONIC LEVEL	FINITE[a] NUCLEUS SOLUTION	FIRST ORDER VACUUM POLAR-IZATION	LAMB SHIFT	HIGHER[b] ORDER VACUUM POLAR-IZATION	NUCLEAR[c] POLAR-IZATION	TOTAL
$1s_{1/2}$	10514.88	66.97	-2.74	1.75	6.8 (12.6)[d]	10587.66 (10593.46)[d]
$2s_{1/2}$	3578.56	19.32	-0.70	0.44	1.6	3599.22
$2p_{1/2}$	4780.45	32.26	-0.35	0.71	1.9	4814.97
$2p_{3/2}$	4598.75	29.74	-0.64	0.64	1.8	4630.39
$3p_{1/2}$	2127.88	10.77	-0.18	0.22	0.7	2139.39
$3p_{3/2}$	2081.10	10.24	-0.13	0.21	0.7	2092.12
$3d_{3/2}$	2162.30	10.51	0.04	0.19	-0.03	2173.01
$3d_{5/2}$	2120.25	9.86	0.05	0.18	0.0	2130.40
$4d_{3/2}$	1213.78	4.58	-0.01	0.05	-	1218.40
$4d_{5/2}$	1196.32	4.33	-0.02	0.05	-	1200.68
$4f_{5/2}$	1197.32	3.80	0.01	0.05	-	1201.19
$4f_{7/2}$	1188.26	3.70	-0.01	0.05	-	1192.01

a) Assumed $\rho_1(r)$ with $c = 1.1235\ A^{1/3}$fm, $n = 12.673$, $m \equiv 1$, $w \equiv 0$.

b) Ref. 13

c) Ref. 6

d) Value obtained from least squares fit to our data.

e) For convenience we have multiplied all binding energies and corrections by -1.

TABLE 2

THEORETICAL POPULATIONS OF MUONIC ^{208}Pb

ATOMIC LEVELS

n/ℓ		0	1	2	3	4
5	j^{a}	0.0010	0.0023	0.0115	0.0651	0.3230
	j'^{b}		0.0013	0.0077	0.0491	0.2590
4	j	0.0024	0.0057	0.0444	0.4075	
	j'		0.0033	0.0300	0.3073	
3	j	0.0023	0.0212	0.4717		
	j'		0.0119	0.3302		
2	j'	0.0161	0.5628			
	j'		0.3095			
1	j	1.00				

a) $j = \ell + 1/2$

b) $j' = \ell - 1/2$

TABLE 3

PHYSICAL PROPERTIES OF ^{208}Pb TARGET

Chemical Form	$Pb(NO_3)_2$
Weight	1600g
Dimensions	14 x 15 x 2 cm
Isotopic Composition-208	98.7%
207	1.0%
206	0.3%

TABLE 4

ENERGY CALIBRATION SOURCES

SOURCE	ENERGY (keV)	PURPOSE
^{46}Sc	889.18 ± 0.10 [a]	^{208}Pb M Feed-Throughs
^{88}Y	897.96 ± 0.10 [a]	M "
^{46}Sc	1120.41 ± 0.10 [a]	M "
^{60}Co	1173.23 ± 0.04 [a]	M "
^{60}Co	1332.48 ± 0.05 [a]	L "
^{88}Y	1836.08 ± 0.07 [a]	L "
^{208}TI (ThC'')	2614.47 ± 0.10 [a]	L "
^{24}Na	2753.92 ± 0.12 [a]	L "
^{66}Ga	4806.58 ± 0.25 [b]	K "
^{56}Co	846.78 ± 0.06 [c]	Linearity and/or efficiency
	1037.90 ± 0.05 [c]	"
	1175.13 ± 0.06 [c]	"
	1238.30 ± 0.04 [c]	"
	1360.24 ± 0.05 [c]	"
	1576.56 ± 0.06 [c]	"
	(2598.57 DE)	

TABLE 4 (Cont.)

SOURCE	ENERGY	PURPOSE
	1771.42 ± 0.07 [c]	Linearity and/or efficiency
	2034.92 ± 0.07 [c]	"
	2087.57 ± 0.06 [c]	"
	(2598.57 SE)	
	2231.64 ± 0.06 [c]	"
	(3253.64 DE)	
	2598.57 ± 0.06 [c]	"
	3253.64 ± 0.06 [c]	"
^{22}Na	1274.55 ± 0.04 [a]	"

[a] Ref. 21

[b] Ref. 22

[c] Ref. 23

TABLE 5

COMPARISON OF ^{208}Pb MUONIC X-RAY ENERGIES

TRANSITION	TYPE	CHICAGO OTTAWA [a] (keV)	CERN [b] (keV)	THIS EXPER. (keV)	THEORY [c] (keV)
$4f_{7/2} \rightarrow 3d_{5/2}$	E1	937.76±0.20 [d]	938.02±0.10 [e]	938.17±0.15	938.23
$4f_{5/2} \rightarrow 3d_{3/2}$	E1	971.74±0.20 [d]	971.88±0.10 [e]	971.99±0.09	971.83
$2s_{1/2} \rightarrow 2p_{3/2}$*	E1	-	-	1031.18±0.46	1031.09
$2s_{1/2} \rightarrow 2p_{1/2}$*	E1	-	-	1216.15±0.78	1215.78
$5f_{7/2} \rightarrow 3d_{5/2}$	E1	-	-	1366.50±0.20	1366.62
$5f_{5/2} \rightarrow 3d_{3/2}$	E1	-	-	1404.52±0.34	1404.69
$3p_{3/2} \rightarrow 2s_{1/2}$*	E1	-	-	1507.18±0.20	1507.22
$3d_{3/2} \rightarrow 2p_{3/2}$*	E1	2456.64±0.47	-	2456.94±0.20	2457.31
$3d_{5/2} \rightarrow 2p_{3/2}$*	E1	2500.07±0.45	-	2500.34±0.19	2500.10
$3d_{3/2} \rightarrow 2p_{1/2}$*	E1	2641.48±0.42	-	2641.94±0.20	2642.00
$4d_{5/2} \rightarrow 2p_{3/2}$ [f]	E1	-	-	3429.24±0.74	3429.64
$4f_{5/2} \rightarrow 2p_{3/2}$ [f]	E2	-	-	-	3429.13
$4f_{7/2} \rightarrow 2p_{3/2}$	E2	-	-	3438.23±0.74	3438.30
$4d_{3/2} \rightarrow 2p_{1/2}$	E1	-	-	3596.78±0.85	3596.52
$4f_{5/2} \rightarrow 2p_{1/2}$	E2	-	-	3613.02±0.84	3613.82
$2p_{1/2} \rightarrow 1s_{1/2}$*	E1	5778.93±0.50	-	5778.5 ±0.5	5778.56
$2p_{3/2} \rightarrow 1s_{1/2}$*	E1	5963.77±0.45	-	5963.3 ±0.5	5963.27
$3d_{3/2} \rightarrow 1s_{1/2}$	E2	-	-	8422.8 ±2.0	8420.58
$3p_{1/2} \rightarrow 1s_{1/2}$	E1	-	-	8454.97±2.1	8454.10
$3d_{5/2} \rightarrow 1s_{1/2}$	E2	-	-	8465.74±2.0	8463.37
$3p_{3/2} \rightarrow 1s_{1/2}$	E1	-	-	8502.90±2.1	8501.59

TABLE 5 (Cont.)

[a]Ref. 8

[b]Ref. 2

[c]These values represent a least squares fit to those transitions marked with an asterisk to a 2 parameter Fermi distribution ρ_1 with $c = 1.1236\ A^{1/3}$fm, $n = 12.69$ and a variable nuclear polarization in the 1s level $\Delta E(1s) = -12.6$ keV.

[d]Values quoted are for ^{206}Pb. The isotope shift in the 3d and 4f levels are 0.1 keV and 0.01 keV respectively.

[e]Values quoted are for natural Pb corrected for isotope shift.

[f]Lines not resolved.

TABLE 6

COMPARISON OF MUONIC X-RAY SPLITTINGS IN ^{208}Pb

SPLITTING	CHICAGO[a] OTTAWA (keV)	THIS EXPER. (keV)	THEORY[b] (keV)
$\Delta 2p$ (K_α)	184.84±0.22	184.87±0.10	184.71
$\Delta 2p$ (2s→2p)	-	184.99±0.35	184.71
$\Delta 2p-\Delta 3d$ (L)	141.41±0.35	141.61±0.26	141.90
$\Delta 3d$ (L)	43.47±0.44[c]	43.39±0.14	42.79
$\Delta 3d$ (3d→1s)	-	42.84±0.32	42.79
$\Delta 3p$ (K_β)	-	47.56±0.82	47.49
$\Delta 3d-\Delta 4f$(M)	33.98±0.10[c]	33.80±0.07	33.60
$\Delta 3d-\Delta 5f$(5f→3d)	-	38.08±0.28	38.07
$\Delta 4f-\Delta 5g$(5g→4f)	6.61±0.20[c]	6.47±0.07	6.41
$\Delta 4f-\Delta 6g$(6g→4f)	-	7.54±0.16	7.59
$\Delta(3d_{5/2}\rightarrow 3p_{3/2})$	-	37.05±0.53	38.22

[a] Reference 8

[b] These values represent a least squares fit to those transitions marked with an asterisk in TABLE 5 and $\Delta 2p(K_\alpha)$ given above to a 2 parameter Fermi distribution ρ_1 with $c = 1.1236A^{1/3}$fm, n= 12.69 and $\Delta E(1s) = -12.6$ keV.

[c] Values quoted are for ^{206}Pb.

TABLE 7

EXPERIMENTAL CONSISTENCY CHECKS

LEVEL DIFFERENCE	TRANSITIONS AND SPLITTINGS USED	TOTAL ENERGY
$3p_{3/2} \rightarrow 2p_{3/2}$	$3p_{3/2} \rightarrow 2s_{1/2} \rightarrow 2p_{3/2}$	2538.36 ± 0.51
	$\Delta(3p_{3/2} - 3d_{5/2})^{a} + 3d_{5/2} \rightarrow 3p_{3/2}$	2537.39 ± 0.56
$3p_{3/2} \rightarrow 2p_{1/2}$	$3p_{3/2} \rightarrow 2s_{1/2} \rightarrow 2p_{1/2}$	2723.33 ± 0.81
	$\Delta(3p_{3/2} - 3d_{5/2})^{a} + \Delta(3d)^{b}$ $+ 3d_{3/2} \rightarrow 2p_{1/2}$	2722.38 ± 0.58
$3d_{5/2} \rightarrow 1s_{1/2}$	$3d_{5/2} \rightarrow 1s_{1/2}$	8465.74 ± 2.0
	$3d_{5/2} \rightarrow 2p_{3/2} \rightarrow 1s_{1/2}$	8463.64 ± 0.54
$3p_{3/2} \rightarrow 1s_{1/2}$	$3p_{3/2} \rightarrow 1s_{1/2}$	8502.9 ± 2.1
	$3p_{3/2} \rightarrow 2s_{1/2} \rightarrow 2p_{1/2} \rightarrow 1s_{1/2}$	8501.66 ± 0.71

[a] Measured splitting between $3p_{3/2} \rightarrow 1s_{1/2}$ and $3d_{5/2} \rightarrow 1s_{1/2}$ transitions.

[b] Measured splitting between $3d_{5/2} \rightarrow 2p_{3/2}$ and $3d_{3/2} \rightarrow 2p_{3/2}$ transitions.

TABLE 8

RELATIVE INTENSITIES OF MUONIC ^{208}Pb TRANSITIONS

TRANSITION	OBSERVED	THEORETICAL
$4f_{7/2} \rightarrow 3d_{5/2}$	0.376 ±0.038	0.393
$4f_{5/2} \rightarrow 3d_{3/2}$	0.270 ±0.027	0.289
$2s_{1/2} \rightarrow 2p_{3/2}$	0.0055±0.001	0.0092
$2s_{1/2} \rightarrow 2p_{1/2}$	0.0047±0.001	0.0069
$5f_{7/2} \rightarrow 3d_{5/2}$	0.039 ±0.004	0.041
$5f_{5/2} \rightarrow 3d_{3/2}$	0.026 ±0.004	0.029
$3p_{3/2} \rightarrow 2s_{1/2}$	0.0065±0.001	0.0088
$3d_{3/2} \rightarrow 2p_{3/2}$	0.054 ±0.007	0.044
$3d_{5/2} \rightarrow 2p_{3/2}$	0.475 ±0.048	0.450
$3d_{3/2} \rightarrow 2p_{1/2}$	0.320 ±0.033	0.255
$4f_{5/2} \rightarrow 2p_{3/2}$ [a]	0.036 ±0.004	0.002
$4d_{5/2} \rightarrow 2p_{3/2}$ [a]		0.030
$4f_{7/2} \rightarrow 2p_{3/2}$	0.014 ±0.002	0.014
$4d_{3/2} \rightarrow 2p_{1/2}$	0.018 ±0.003	0.018
$4f_{5/2} \rightarrow 2p_{1/2}$	0.0075±0.0016	0.0071

[a] Lines not resolved.

TABLE 9

RELATIVE INTENSITIES OF MUONIC

^{208}Pb FINE STRUCTURE COMPONENTS OF PRINCIPAL TRANSITIONS

	Chicago Ottawa[a]	This Experiment	Theory
$R_p = \frac{2p_{3/2} \rightarrow 1s_{1/2}}{2p_{1/2} \rightarrow 1s_{1/2}}$	1.64 ± 0.06	1.67 ± 0.07	1.82
$R_d = \frac{3d_{5/2} \rightarrow 2p_{3/2}}{3d_{3/2} \rightarrow 2p_{1/2}}$	1.61 ± 0.09	1.53 ± 0.03	1.77
$R_{d1} = \frac{3d_{5/2} \rightarrow 2p_{3/2}}{3d_{3/2} \rightarrow 2p_{3/2}}$	10.8 ± 3.0	8.33 ± 0.58	10.2
$R_f = \frac{4f_{7/2} \rightarrow 3d_{5/2}}{4f_{5/2} \rightarrow 3d_{3/2}}$	1.35 ± 0.05	1.36 ± 0.02	1.36

[a]Reference 8

TABLE 10

INTENSITIES OF FINE STRUCTURE COMPONENTS

FOR ^{208}Pb $\Delta n>1$ TRANSITIONS

TRANSITION	OBSERVED	THEORETICAL[a]
$4f_{7/2} \rightarrow 2p_{3/2}$	1371 ± 136	1417
$4f_{5/2} \rightarrow 2p_{1/2}$	641 ± 120	686
$4d_{5/2} \rightarrow 2p_{3/2}$[b]	3463 ± 195	3035
$4f_{5/2} \rightarrow 2p_{3/2}$[b]		193
$4d_{3/2} \rightarrow 2p_{1/2}$	1554 ± 166	1730
$3d_{5/2} \rightarrow 1s_{1/2}$	1089 ± 80	1136
$3d_{3/2} \rightarrow 1s_{1/2}$	693 ± 57	696
$3p_{3/2} \rightarrow 1s_{1/2}$	408 ± 60	676
$3p_{1/2} \rightarrow 1s_{1/2}$	354 ± 55	304

[a]The predicted $4 \rightarrow 2$ intensities are normalized to the observed intensities, the $3 \rightarrow 1$ transitions are normalized excluding the $3p_{3/2} \rightarrow 1s_{1/2}$.

[b]Lines not resolved.

TABLE 11

SENSITIVITY OF ^{208}Pb CHARGE PARAMETERS TO POLARIZATION

ASSUMPTIONS FOR 2-PARAMETER FERMI DISTRIBUTION

Assumption	i) No Nuclear Polarization	ii) Skardhamar[b] Polarization	iii) Skardhamar Polarization with variable ΔE(ls)
$C/A^{1/3}$ (fm)	1.1258±0.0006	1.1203±0.0007	1.1236±0.0009
n	13.20±0.06	12.46±0.07	12.69±0.08
t (fm)	2.223±0.010	2.346±0.013	2.312±0.014
ΔE(ls) (keV)	0[a]	-6.8[a]	-12.6±0.8
$r_o/A^{1/3}$ (fm)	1.1979	1.2005	1.2012
χ^2/DF	30.8/7	59.5/6	8.7/6

[a] Held constant

[b] Reference 6

TABLE 12

COMPARISON OF ^{208}Pb CHARGE PARAMETERS

FOR FERMI-LIKE DISTRIBUTIONS

(3-PARAMETER FITS)

Distribution	ρ_1 (1)	ρ_1 (2)	ρ_1 (3)	ρ_2 (4)
$C/A^{1/3}$ (fm)	1.1236±0.0009	1.1022±0.0009	1.0652±0.0013	1.0943±0.0011
n	12.69±0.08	12.07±0.09	2.177±0.009	2.171±0.008
w	0 [a]	0.14 [a]	0.3379 [a]	0.361 [a]
m	1 [a]	1 [a]	2 [a]	2 [a]
$\Delta E(1s)$ (keV)	-12.6±0.8	-12.6±0.9	-12.5±0.8	-12.5±0.8
$r_o/A^{1/3}$ (fm)	1.2012	1.2013	1.2012	1.2013
χ^2 [b]	8.7	8.4	8.8	8.3

[a] Held constant

[b] For 6 degrees of freedom.

TABLE 13

COMPARISON OF ^{208}Pb CHARGE PARAMETERS

FOR FERMI-LIKE DISTRIBUTIONS

(4-PARAMETER FITS)

Distributions	ρ_1	ρ_1	ρ_1	ρ_2
$c/A^{1/3}$ (fm)	1.1193±0.0027	1.0978±0.0029	1.0589±0.0044	1.0888±0.0036
n	12.33±0.21	11.77±0.19	2.142±0.024	2.137±0.023
w [a]	0	0.14	0.3379	0.361
m [a]	1	1	2	2
ΔE(1s) (keV)	-8.9±2.3	-9.1±2.4	-8.9±2.6	-8.8±2.4
ΔE(2s) (keV)	-0.56±0.62	-0.69±0.65	-0.60±0.69	-0.53±0.55
$r_o/A^{1/3}$ (fm)	1.201	1.201	1.201	1.201
χ^2 [b]	5.99	6.05	6.08	6.03

[a] Held constant

[b] For 5 degrees of freedom

TABLE 14

NUCLEAR POLARIZATION IN MUONIC ^{208}Pb

	Theory		Experiment
Level	Chen	Skardhamar	
$1s_{1/2}$	-6.0±0.6	-6.8±2.0	-8.9±2.7
$2s_{1/2}$	-1.2±0.2	-1.6±0.7	-0.6±0.7

TABLE 15

COMPARISON OF MUONIC X RAY AND ELECTRON SCATTERING INTERPRETATIONS

Distribution	Electron Scattering [a] ρ_1	This Exp. ρ_1	Electron Scattering [c] ρ_1	This Exp. ρ_1
$c/A^{1/3}$ (fm)	1.08±0.01	1.098±0.015	1.059	1.044±0.008
n	11.81±0.20	11.77±0.40	2.156	2.094±0.024
w	0.14±0.10	0.14±0.10 [b]	0.4345	0.4345±0.05 [b]
m	1	1	2	2

[a] Reference 29

[b] Assumed electron scattering value and error

[c] Reference 15

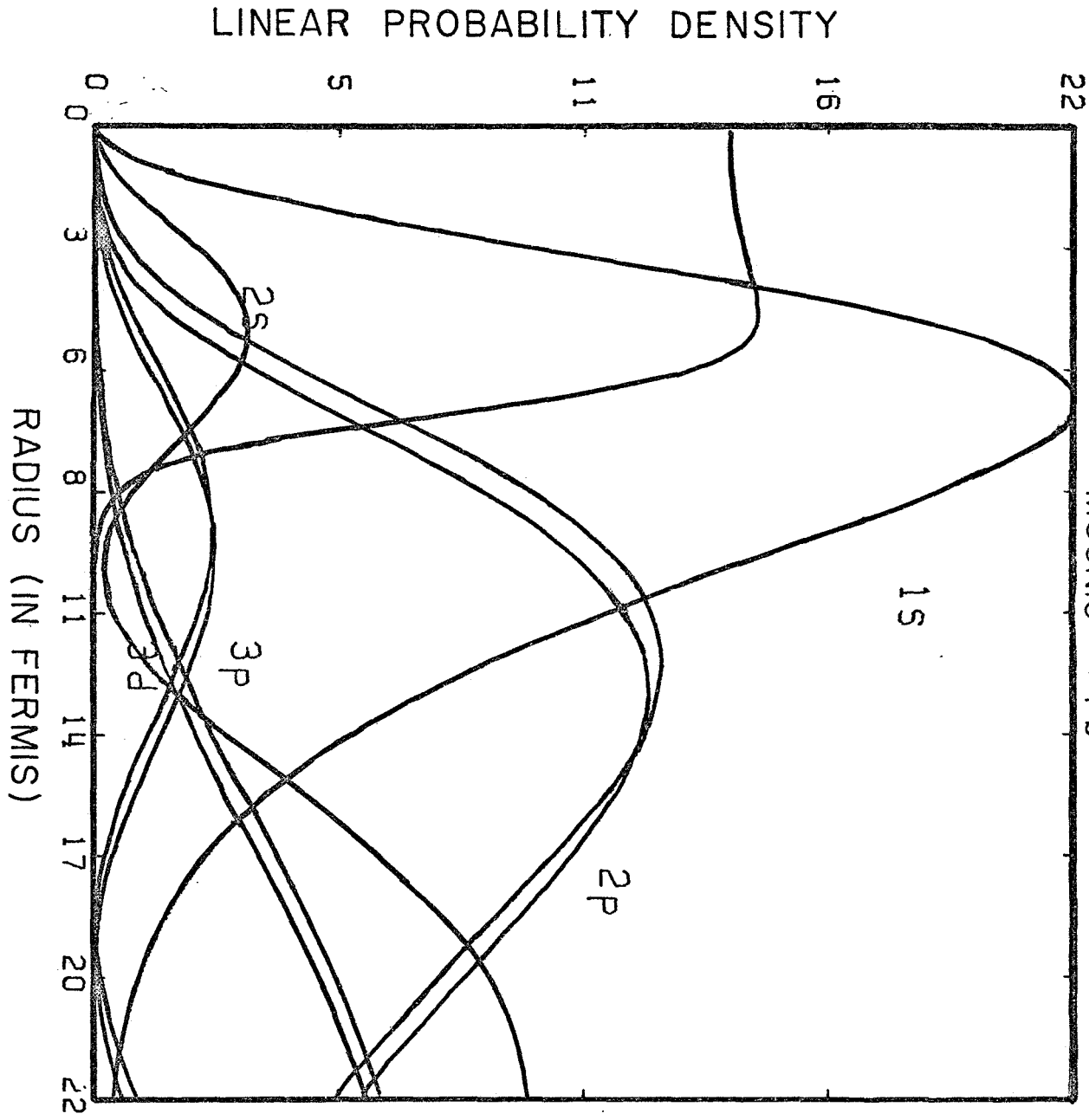
LINEAR PROBABILITY DENSITY
0
5
11
16
22
0
3
6
8
11
14
17
20
22
RADIUS (IN FERMIS)
MUONIC ^{208}Pb
1S
2S
2P
3P
3D

Fig. 1

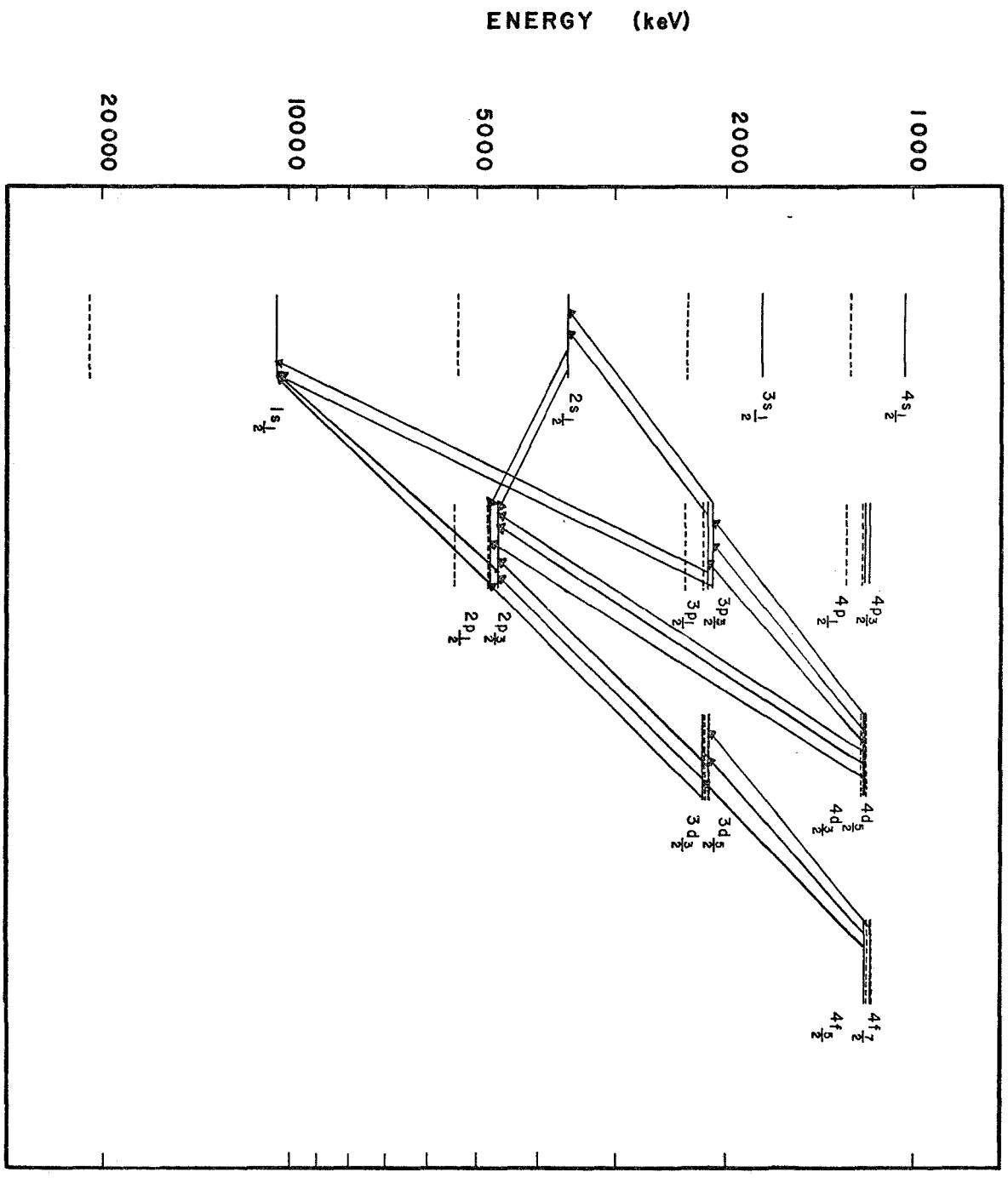
ENERGY (keV)
20000
10000
5000
2000
1000
MUONIC ENERGY LEVELS IN 208Pb
1s 1/2
2s 1/2
2p 1/2
2p 3/2
3s 1/2
3p 1/2
3p 3/2
3d 3/2
3d 5/2
4s 1/2
4p 1/2
4p 3/2
4d 3/2
4d 5/2
4f 5/2
4f 7/2

Fig. 2

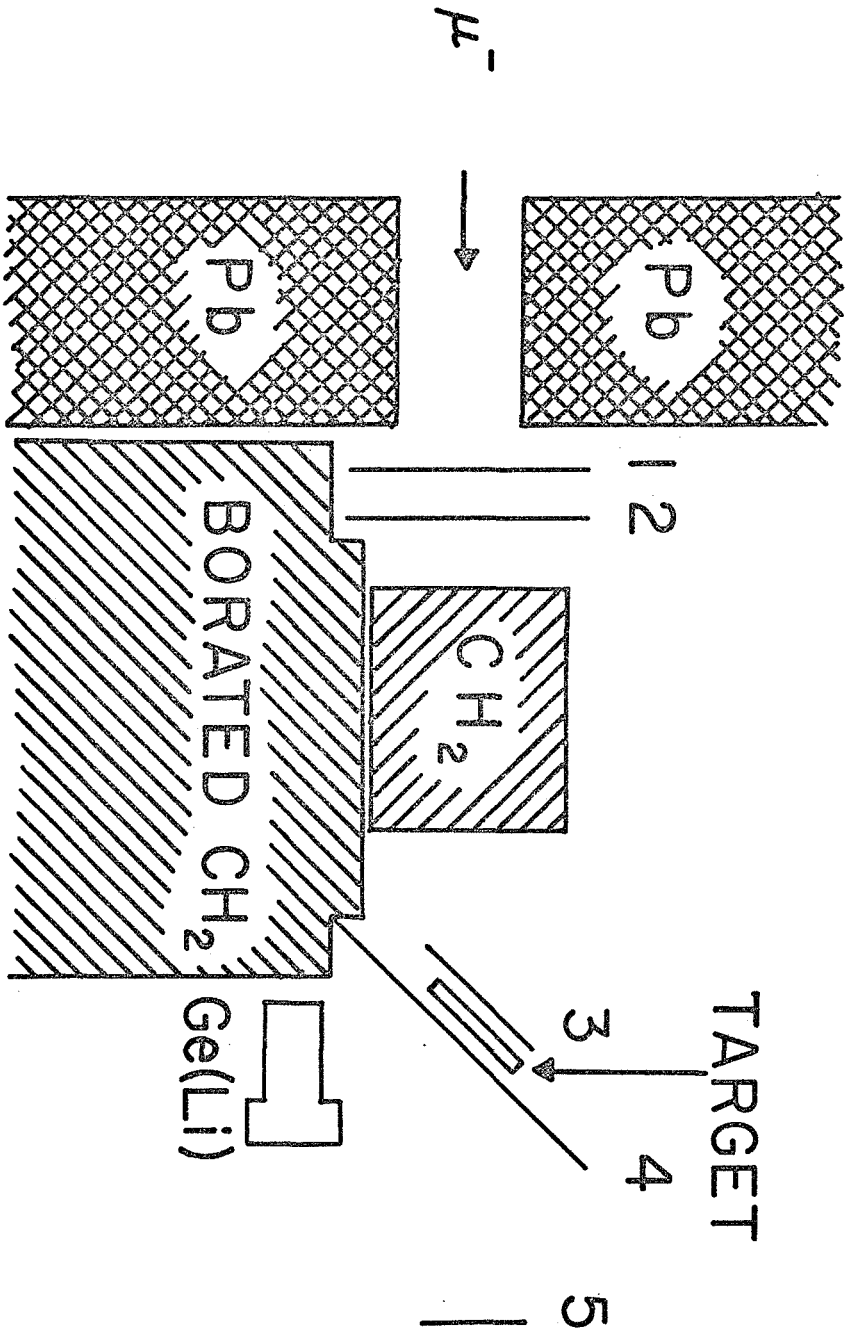

Fig. 3

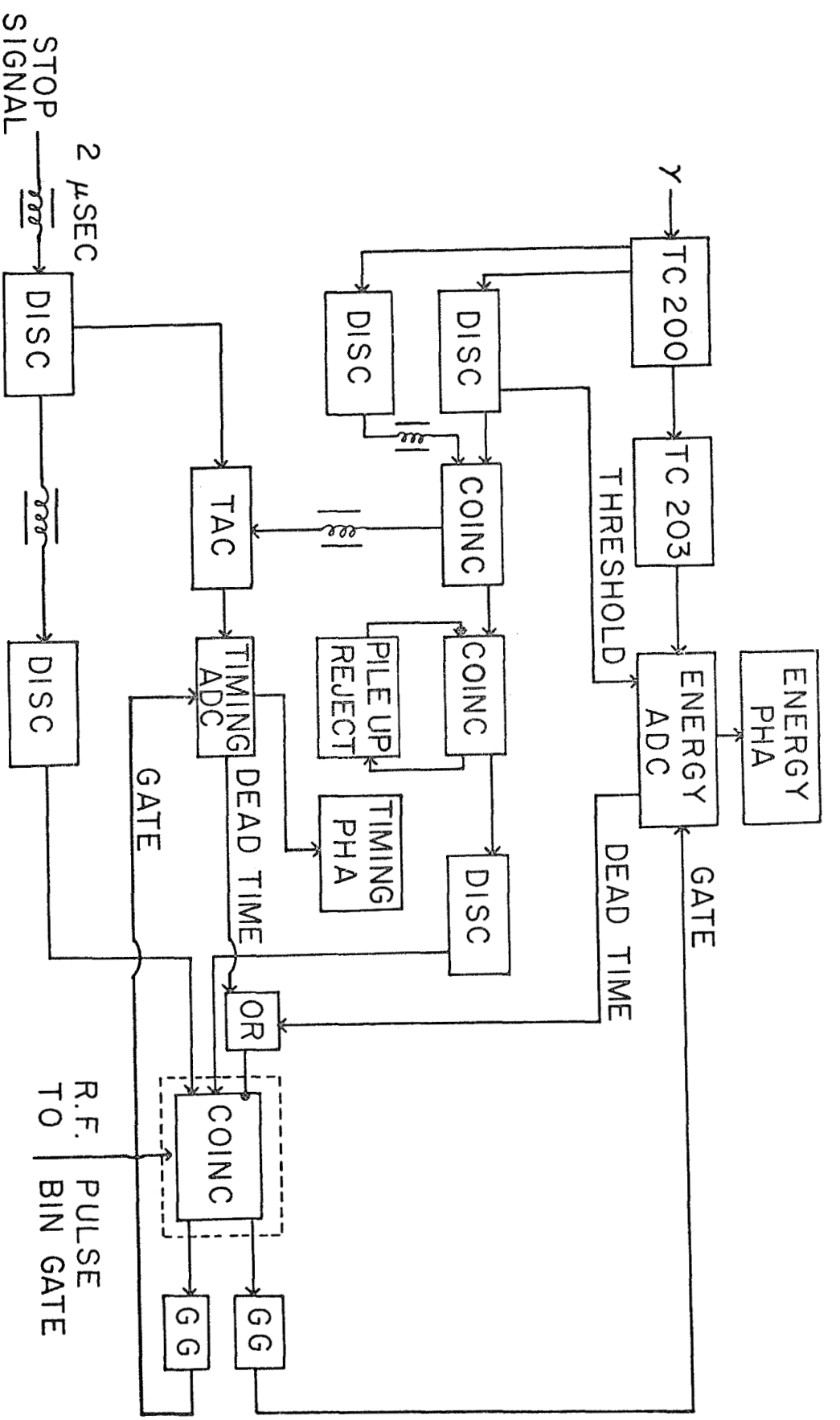
γ
TC 200
TC 203
ENERGY PHA
ENERGY ADC
THRESHOLD
GATE
DEAD TIME
DISC
DISC
COINC
TAC
COINC
PILE UP REJECT
TIMING ADC
TIMING PHA
DISC
GATE
DEAD TIME
OR
COINC
R.F. TO PULSE BIN GATE
G G
G G
STOP SIGNAL
2 μSEC
DISC
DISC

Fig. 4

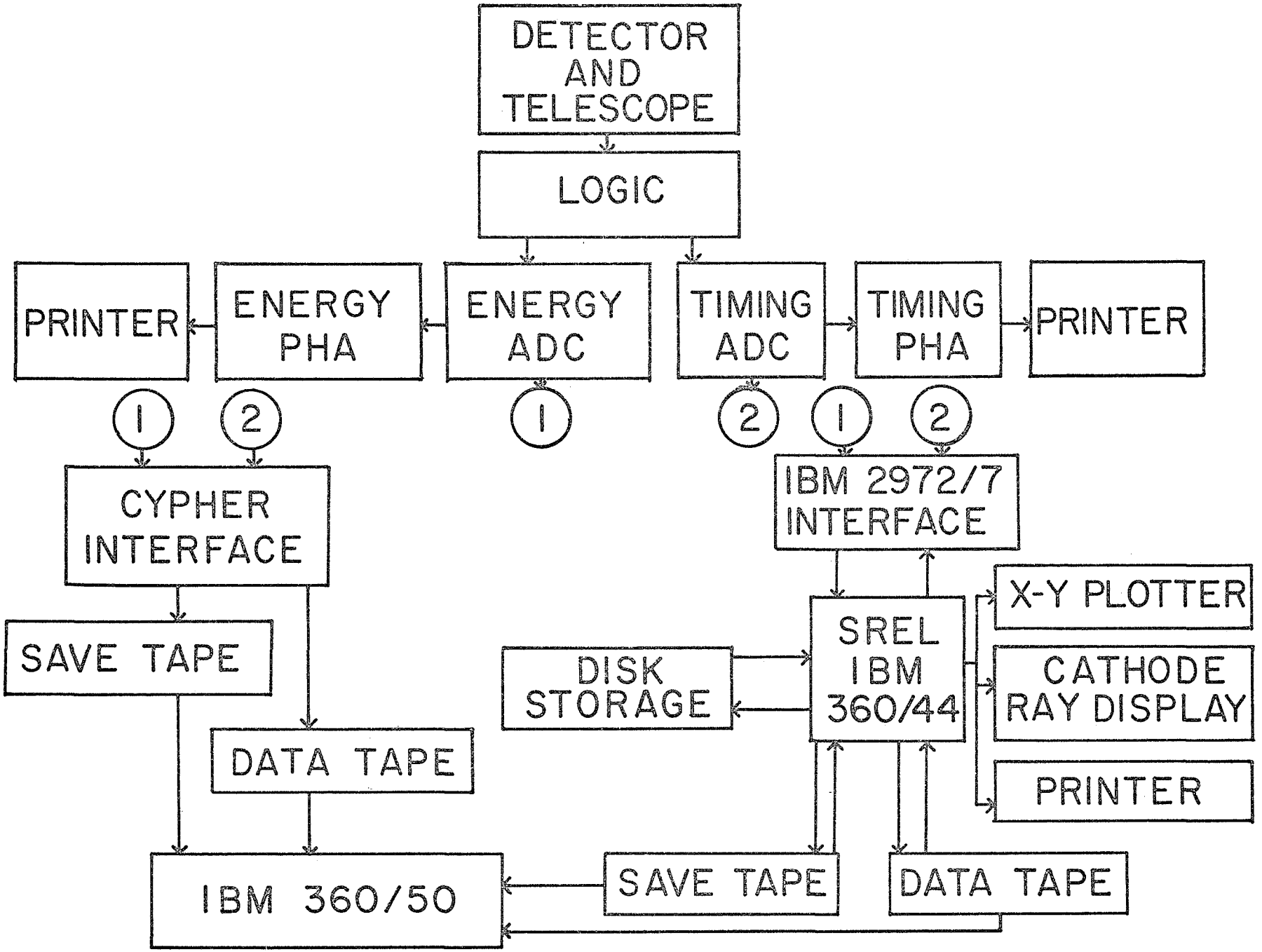
DETECTOR AND TELESCOPE
LOGIC
PRINTER
ENERGY PHA
ENERGY ADC
TIMING ADC
TIMING PHA
PRINTER
1
2
1
2
1
2
CYPHER INTERFACE
IBM 2972/7 INTERFACE
SAVE TAPE
DATA TAPE
DISK STORAGE
SREL IBM 360/44
X-Y PLOTTER
CATHODE RAY DISPLAY
PRINTER
IBM 360/50
SAVE TAPE
DATA TAPE

Fig. 5

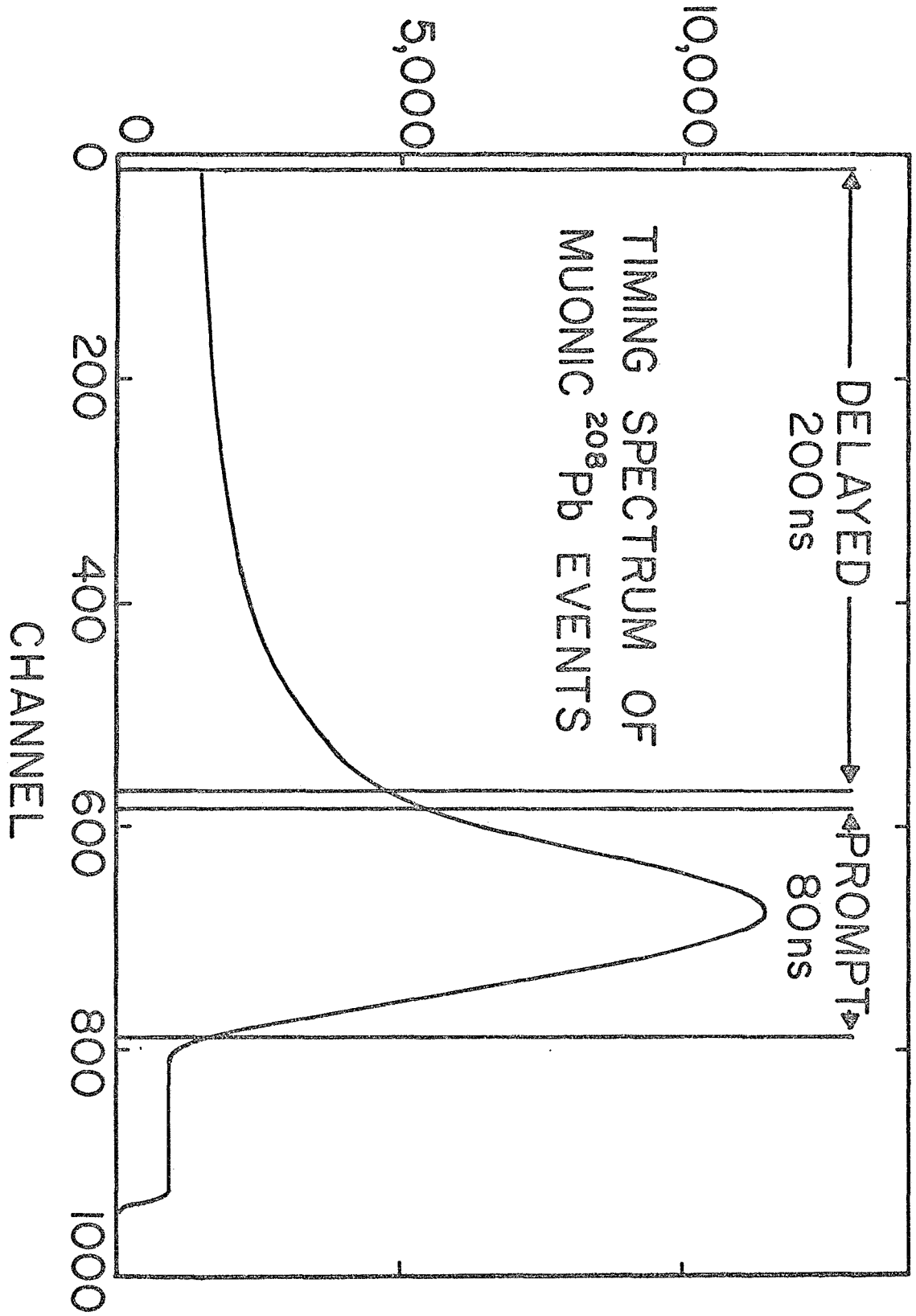
COUNTS / CHANNEL
0
5,000
10,000
CHANNEL
0
200
400
600
800
1000
TIMING SPECTRUM OF
MUONIC ^{208}Pb EVENTS
DELAYED
200ns
PROMPT
80ns

Fig. 6

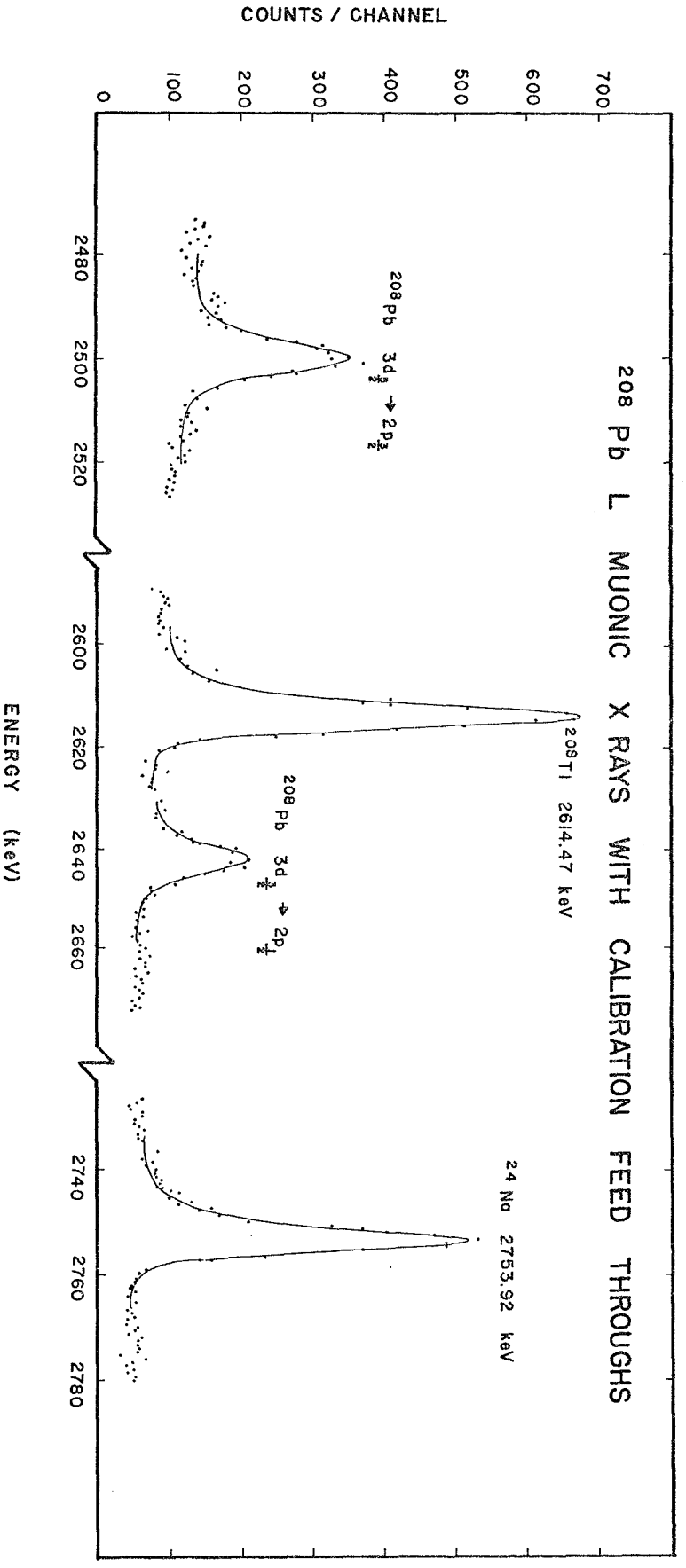
COUNTS / CHANNEL
208 Pb L MUONIC X RAYS WITH CALIBRATION FEED THROUGHS
208 Pb 3d3/2 → 2p3/2
208Tl 2614.47 keV
208 Pb 3d3/2 → 2p1/2
24 Na 2753.92 keV
ENERGY (keV)

Fig. 7

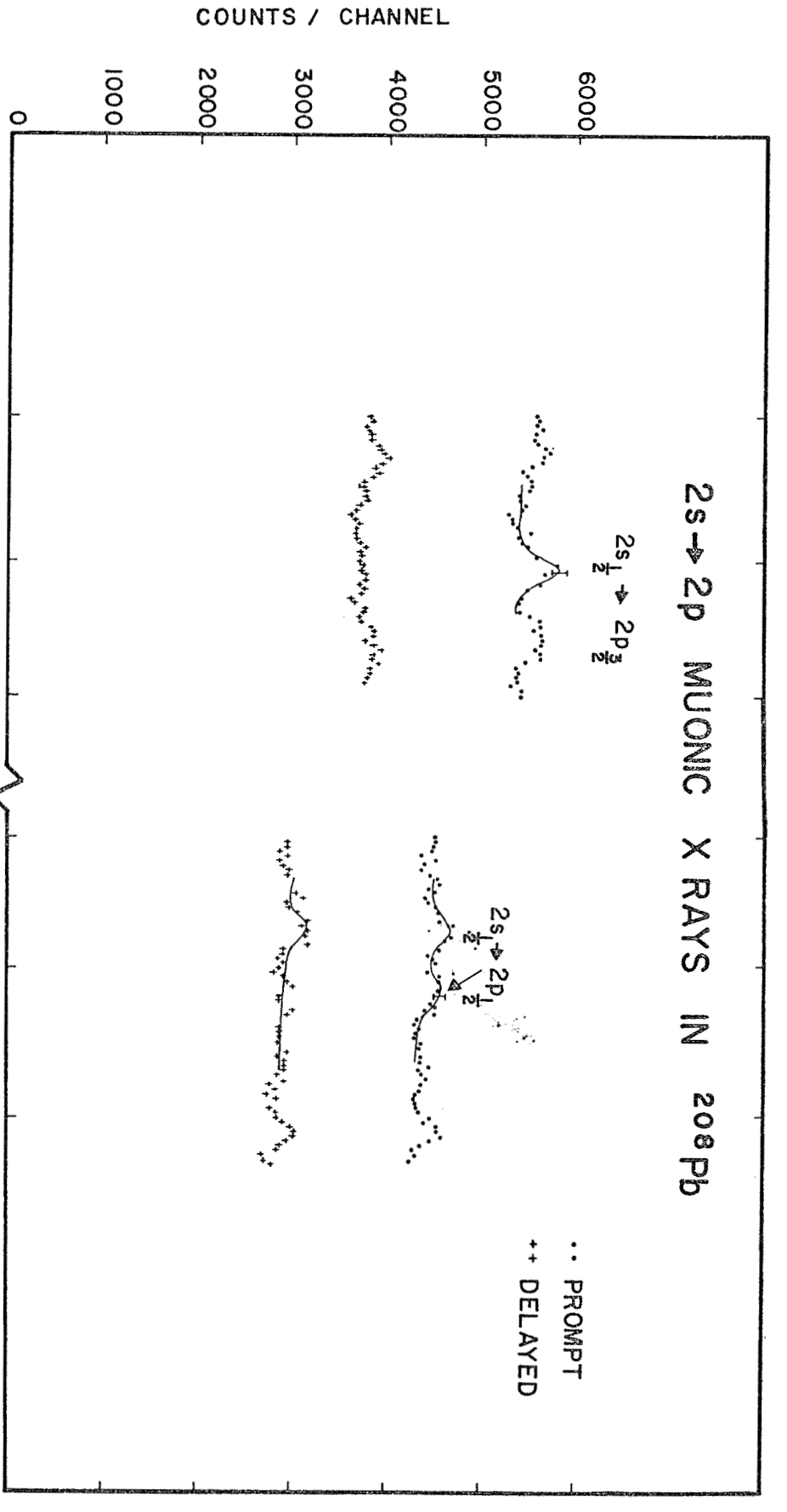
COUNTS / CHANNEL
0
1000
2000
3000
4000
5000
6000
1010
1030
1050
1200
1220
1240
ENERGY (keV)
2s → 2p MUONIC X RAYS IN 208Pb
$2s_{\frac{1}{2}} \rightarrow 2p_{\frac{3}{2}}$
$2s_{\frac{1}{2}} \rightarrow 2p_{\frac{1}{2}}$
·· PROMPT
++ DELAYED

Fig. 8

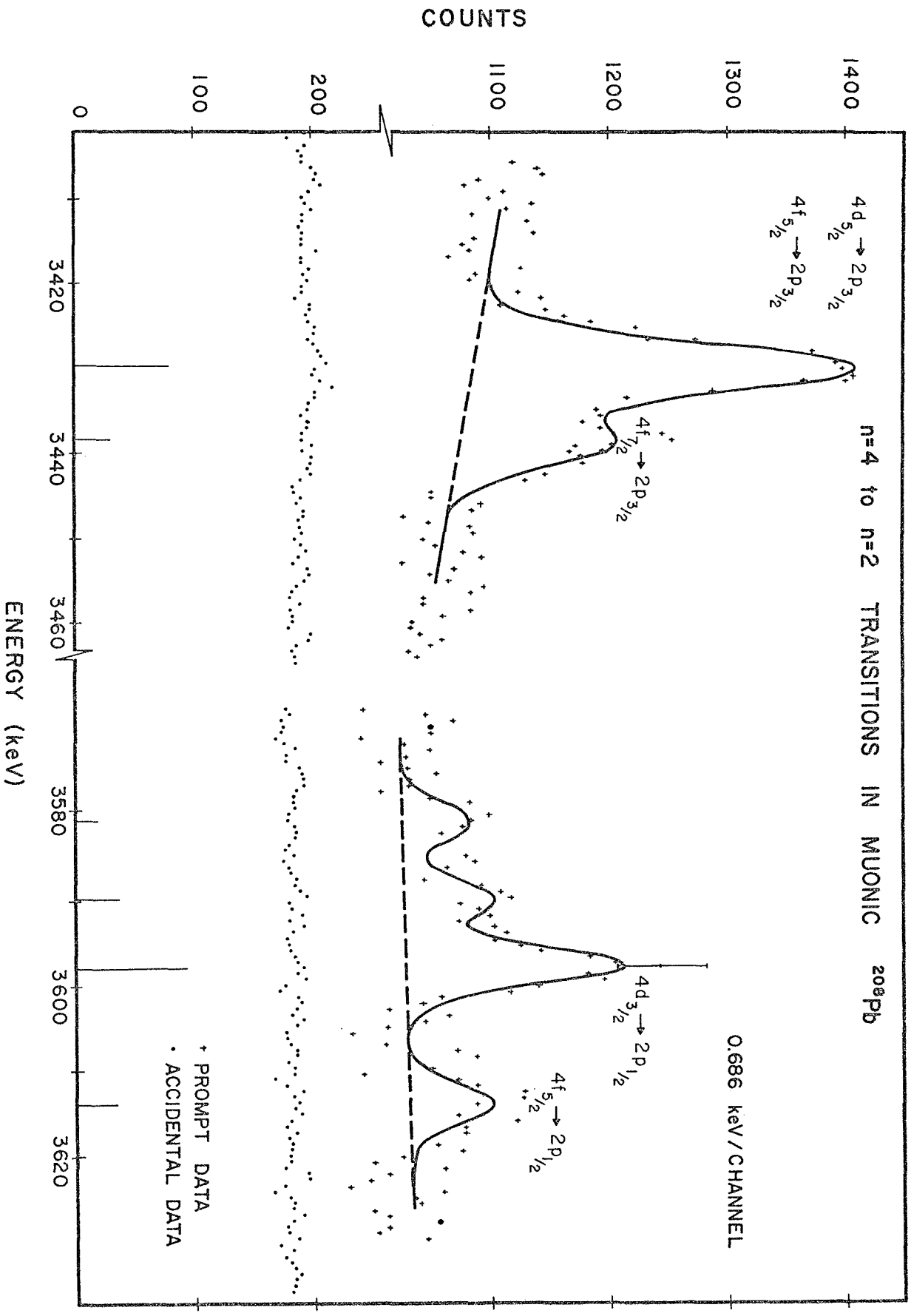
COUNTS
1400
1300
1200
1100
200
100
0
3420
3440
3460
3580
3600
3620
ENERGY (keV)
n=4 to n=2 TRANSITIONS IN MUONIC 208Pb
0.686 keV/CHANNEL
4d5/2 → 2p3/2
4f5/2 → 2p3/2
4f7/2 → 2p3/2
4d3/2 → 2p1/2
4f5/2 → 2p1/2
+ PROMPT DATA
• ACCIDENTAL DATA

Fig. 9

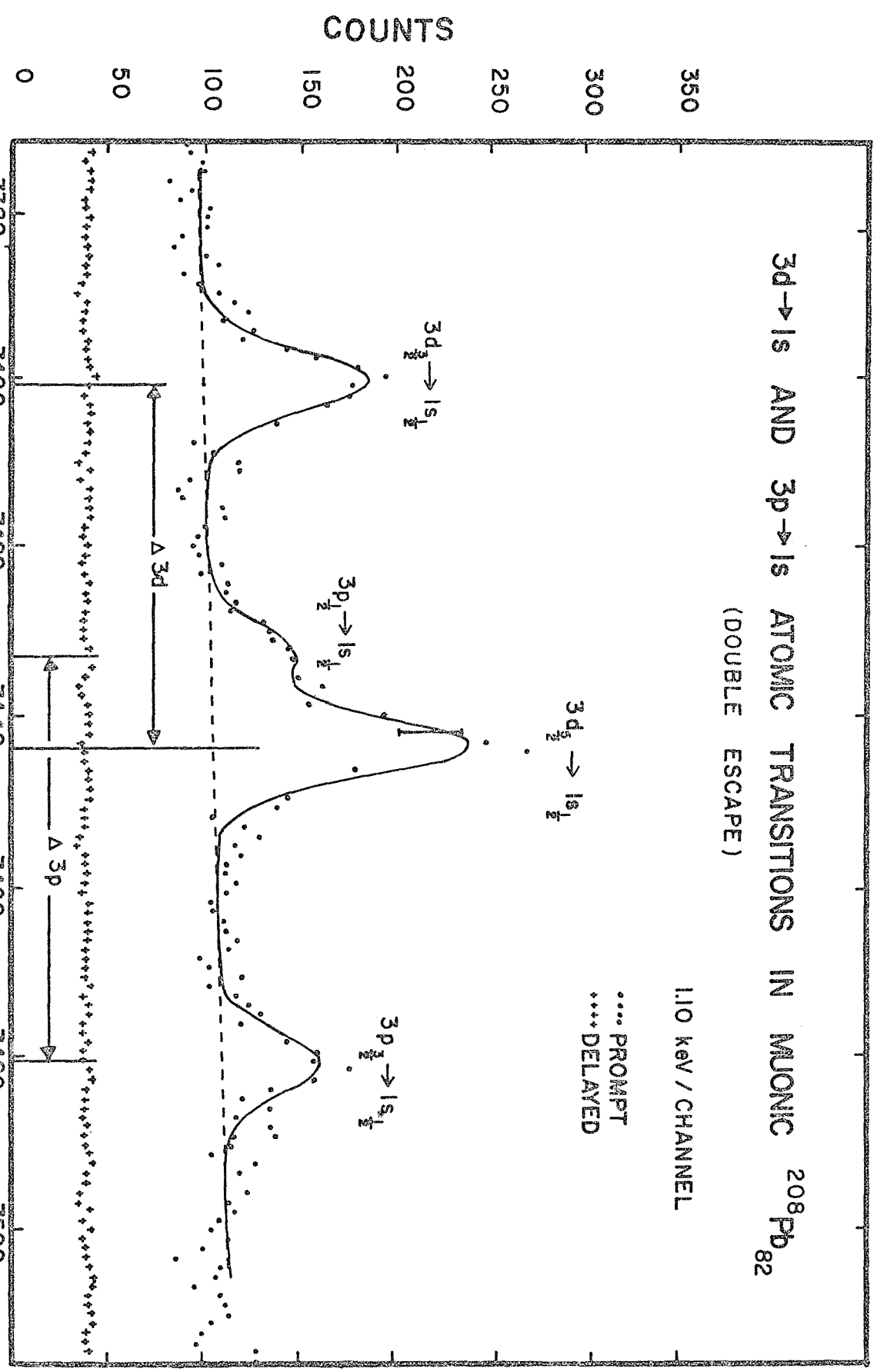
3d → 1s AND 3p → 1s ATOMIC TRANSITIONS IN MUONIC $^{208}Pb_{82}$
(DOUBLE ESCAPE)
1.10 keV / CHANNEL
PROMPT
DELAYED
COUNTS
ENERGY (keV)
$3d_{\frac{3}{2}} \rightarrow 1s_{\frac{1}{2}}$
$3p_{\frac{1}{2}} \rightarrow 1s_{\frac{1}{2}}$
$3d_{\frac{5}{2}} \rightarrow 1s_{\frac{1}{2}}$
$3p_{\frac{3}{2}} \rightarrow 1s_{\frac{1}{2}}$
Δ 3d
Δ 3p
0
50
100
150
200
250
300
350
7380
7400
7420
7440
7460
7480
7500

Fig. 10

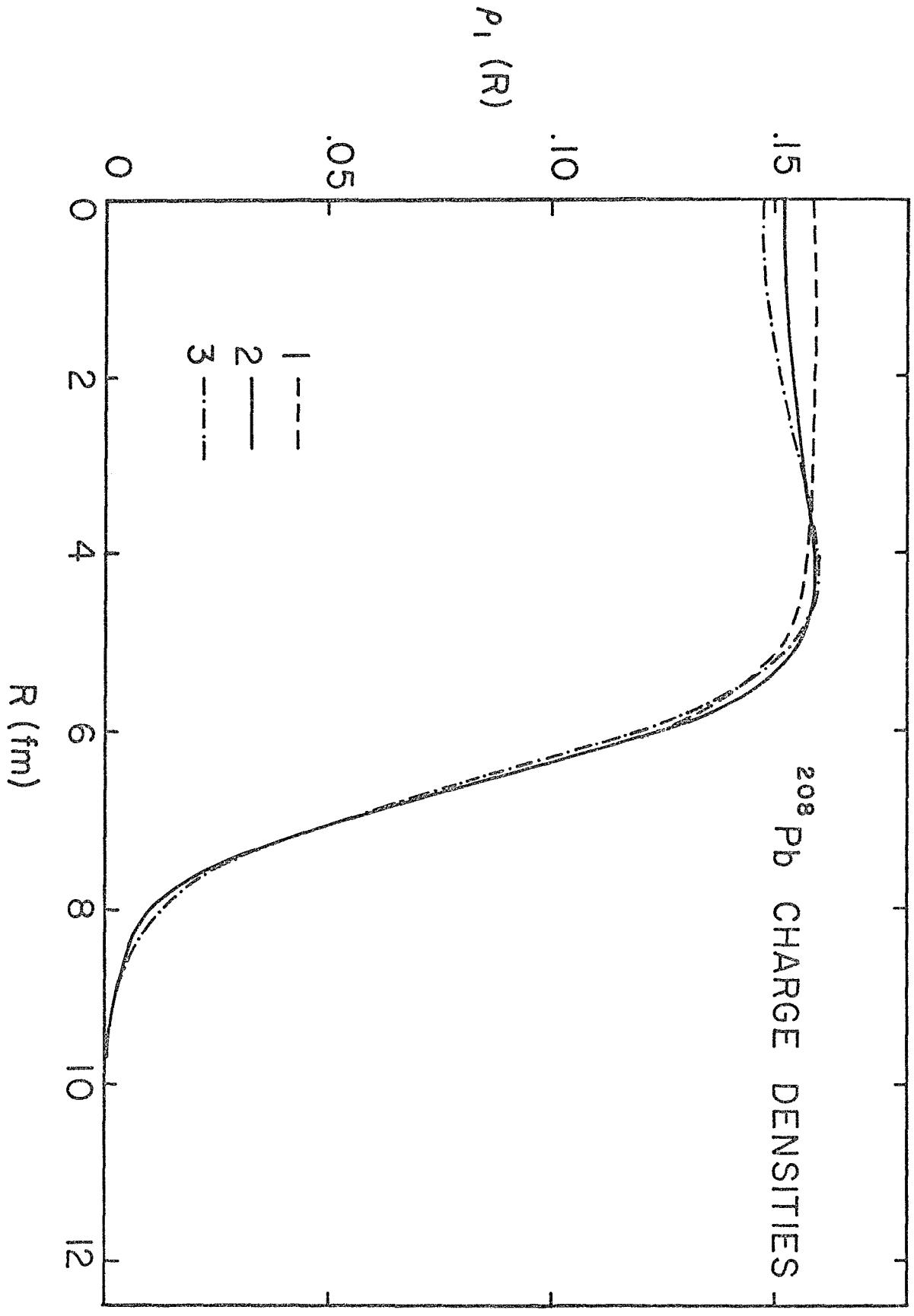

Fig. 11